The Company of **Biologists**

RESEARCH ARTICLE

The Mre11-Rad50-Nbs1 complex mediates the robust recruitment of Polo to DNA lesions during mitosis in *Drosophila*

Cedric Landmann*, Priscillia Pierre-Elies*, Damien Goutte-Gattat, Emilie Montembault, Marie-Charlotte Claverie and Anne Royou‡

ABSTRACT

The DNA damage sensor Mre11-Rad50-Nbs1 complex and Polo kinase are recruited to DNA lesions during mitosis. However, their mechanism of recruitment is elusive. Here, using live-cell imaging combined with micro-irradiation of single chromosomes, we analyze the dynamics of Polo and Mre11 at DNA lesions during mitosis in *Drosophila*. These two proteins display distinct kinetics. Whereas Polo kinetics at double-strand breaks (DSBs) are Cdk1-driven, Mre11 promptly but briefly associates with DSBs regardless of the phase of mitosis and re-associates with DSBs in the proceeding interphase. Mechanistically, Polo kinase activity is required for its own recruitment and that of the mitotic proteins BubR1 and Bub3 to DSBs. Moreover, depletion of Rad50 severely impaired Polo kinetics at mitotic DSBs. Conversely, ectopic tethering of Mre11 to chromatin was sufficient to recruit Polo. Our study highlights a novel pathway that links the DSB sensor Mre11-Rad50-Nbs1 complex and Polo kinase to initiate a prompt, decisive response to the presence of DNA damage during mitosis.

KEY WORDS: Mitosis, *Drosophila*, DNA damage, Polo, BubR1, Bub3, Mre11, Rad50, Checkpoint, Chromosomes, Anaphase, ACP/C, Cdc20, DNA double strand breaks

INTRODUCTION

Cells encounter genotoxic stress originating from extrinsic and intrinsic sources (Cannan and Pederson, 2016). DNA double-strand breaks (DSBs) are potentially the most harmful damage as they can cause genomic instability, a hallmark of cancer cells (Jackson and Bartek, 2009). The presence of DSBs in interphase triggers a conserved signaling pathway, also known as the DNA damage response (DDR), that promotes DNA repair concomitantly with cell cycle delay through checkpoint activation (Hartlerode and Scully, 2009; Melo and Toczyski, 2002; Sekelsky, 2017). In brief, DSBs are promptly recognized by DNA damage sensors including the conserved proteins Meiotic recombination 11 homolog 1 (Mre11) and Rad50, which are part of a complex with the less-conserved Nijmegen breakage syndrome protein 1 (Nbs1; also called Nbn) (Lisby et al., 2004; Lukas et al., 2003, 2004; Syed and Tainer, 2018; Williams et al., 2010). Subsequently, the Mre11-Rad50-Nbs1 (MRN) complex

recruits the phosphoinositide-3-kinase-related kinase (PIKK) Ataxia telangiectasia mutated (ATM) to the site of DNA damage via direct interactions (Falck et al., 2005). ATM promotes the rapid modification of chromatin flanking the breaks, including extensive phosphorylation of the histone 2A variant H2AX (Rogakou et al., 1998), which serve as docking sites for the C-terminal motif of Breast cancer type 1 susceptibility protein present in Mediator of DNA damage checkpoint protein 1 (MDC1) (Dronamraju and Mason, 2009; Stewart et al., 2003; Stucki et al., 2005). MDC1 directly interacts with Nbs1 and recruits additional MRN complexes to DSBs via an amplification loop (Lukas et al., 2004; Wu et al., 2008). This primary signal is transduced to effectors that direct DNA repair through two main pathways: the error-prone non-homologous end-joining (NHEJ) pathway or the error-free homologous recombination (HR) pathway (Ceccaldi et al., 2016; Syed and Tainer, 2018).

Studies have reported a variety of responses to the presence of DSBs during mitosis, depending on the stage at which the damage occurs (Blackford and Stucki, 2020; Thompson et al., 2019). A single broken chromosome end created by the breakage of a dicentric chromosome during anaphase can produce a chromosomal breakage–fusion–bridge cycle (McClintock, 1938). It can also be repaired by either *de novo* telomere formation or homolog-dependent restoration of the chromosome terminus (Ahmad and Golic, 1998; Bhandari et al., 2019; Haber and Thorburn, 1984; McClintock, 1939, 1941). In budding yeast, a DSB created during telophase triggers reversion of chromosome segregation and coalescence of sister chromatids that facilitates repair by HR (Ayra-Plasencia and Machín, 2019). In vertebrates, the presence of DSBs in prometaphase activates primary DNA damage signaling, comprising DNA lesion recognition by the MRN complex followed by partial activation of ATM and subsequent H2AX phosphorylation on chromatin proximal to the breaks (Benada et al., 2015; Giunta et al., 2010; Gomez-Godinez et al., 2010; Orthwein et al., 2014; Peterson et al., 2011; Silva et al., 2014; Terasawa et al., 2014). Subsequent downstream signaling pathways that promote DNA repair by NHEJ and HR are inhibited until the next G1 phase (Benada et al., 2015; Giunta et al., 2010; Orthwein et al., 2014; Peterson et al., 2011; Terasawa et al., 2014; van Vugt et al., 2010; Yu et al., 2012). In *Drosophila* neuroblasts, clustered DSBs on one chromosome are recognized by the mitotic proteins Polo, BubR1 and Bub3. These proteins mediate the proper segregation of the damaged chromatid by tethering the two broken ends (Derive et al., 2015; Royou et al., 2010).

BubR1 and Bub3 act together to stabilize kinetochore–microtubule attachments. They also participate in the spindle assembly checkpoint, which inhibits the anaphase-promoting complex/cyclosome (APC/C), an E3 ubiquitin ligase that triggers anaphase by targeting key substrates for proteolysis, until all

chromosomes are properly attached to the spindle (Basu et al., 1999, 1998; Karess et al., 2013; Lopes et al., 2005). In a recent study, we provided evidence that BubR1 and Bub3 depend on each other to localize on DNA lesions during mitosis where they promote local inhibition of the APC/C via sequestration of the APC/C cofactor Cdc20 (Fzy in *Drosophila*) (Derive et al., 2015).

Polo is a serine/threonine kinase that plays multiple conserved functions during mitosis, including centrosome maturation, bipolar spindle formation, kinetochore function and cytokinesis (Archambault et al., 2015; Llamazares et al., 1991; Sunkel and Glover, 1988). We found that Polo participates in a signaling pathway that tethers chromosome fragments during mitosis, thus preventing genome instability (Royou et al., 2010). However, the molecular pathway governing Polo, BubR1 and Bub3 recruitment to broken chromosomes and their dependency relationship with the DNA damage signaling pathway identified in vertebrate mitotic cells has not been characterized.

In this study, we examined the kinetics of *Drosophila* Polo, BubR1 and Bub3 at DNA lesions created with a pulsed-UV laser in a precise spatiotemporal manner during the different phases of mitosis to assess the coordination of their recruitment to DSBs and investigated their interplay with the DSB sensor (the MRN complex).

RESULTS

Polo is promptly recruited to DNA lesions during mitosis and its kinetics are coupled to Cdk1 activity

The kinetics of Polo recruitment to DSBs in mitosis were first examined by inducing surgical damage to one chromosome in live *Drosophila* neuroblasts at precise times during mitosis with a pulsed-UV laser. The signal of GFP::Polo on the resulting DNA lesions was subsequently monitored by time-lapse imaging (within 1-5 s of irradiation). This method of micro-irradiation (IR) creates complex DNA lesions including DSBs (Aleksandrov et al., 2018). We first calibrated laser power to determine the optimal IR dose for our experiments. We identified 20% laser power as the lowest dose that produced a 100% response (i.e. the presence of a detectable Polo signal at the site of damage) (Fig. S1A-D). In contrast to 20% laser power, lower IR doses resulted in a dramatic decrease in the frequency of cells exhibiting a detectable GFP::Polo signal at the lesions and a significant delay in the appearance of GFP::Polo, accompanied by reduced levels of GFP-Polo at the site of damage (Fig. S1A-D). Because no noticeable changes in GFP::Polo kinetics were observed between 20 and 30% power, we chose to induce DSBs using 20% laser power in all subsequent experiments. This response was specific to damage on the chromosomes as no GFP::Polo foci were detected in the cytoplasm after IR (Fig. S1E).

Because Polo is targeted to different subcellular structures depending on the stage of mitosis, we reasoned that its recruitment to DSBs could be dependent upon the stage of mitosis during which DSBs were created. We therefore measured the kinetics of GFP::Polo on DSBs induced at different phases of mitosis. Cells were irradiated in prometaphase (after nuclear envelope breakdown and at least 2 min before anaphase onset), metaphase (less than 2 min before anaphase onset), anaphase (within 2 min of anaphase onset) and telophase/G1 (>6 min after anaphase onset, during chromatin decondensation and nuclear expansion). Following IR, Polo signal was consistently detected at the site of DNA damage when the damage was induced during prometaphase, metaphase and anaphase (Fig. 1A). By contrast, no GFP::Polo signal or only traces were detected at the site of IR-

induced damage at telophase/G1 phase (T/G1) (Fig. 1A,C,F). In most cases, Polo exhibited biphasic kinetics at DSBs, with a period of accumulation followed by a period of dissociation. In some instances, a short plateau was observed between the phases of association and dissociation (Fig. 1B, PM curve). Polo signal was detected on DSBs 20-40 s following IR during all stages except T/G1 (Fig. 1C). Its half-time recruitment was variable (ranging from 1 to >6 min), particularly when IR was applied during prometaphase (Fig. 1D), and was correlated with the time elapsed between IR and anaphase onset ($R^2=0.5$, Fig. S2A). Importantly, Polo onset of dissociation from the damaged chromatin consistently occurred near or after anaphase onset, in concert with Cyclin-dependent kinase 1 (Cdk1) inhibition (Fig. 1B,E). The maximum levels of Polo at DNA lesions varied between cells, but did not correlate with the time elapsed between IR and anaphase onset (Fig. 1F and Fig. S2B). However, Polo never reached high levels on lesions induced after anaphase onset (Fig. 1F). We noted that a pool of Polo remained associated with DSBs more than 6 min following anaphase onset, which corresponds to the average time of completion of nuclear envelope re-formation in *Drosophila* neuroblasts (Fig. 1A, last images in each panel) (Montembault et al., 2017). We conclude that Polo is rapidly recruited to DNA lesions encountered at any point during mitosis and that the efficiency of its recruitment to DSBs correlates with Cdk1 activity.

Because Polo dissociation from DNA lesions consistently occurred after sister chromatid separation, at a time of Cdk1 inhibition, we determined whether Polo maintenance at DSBs correlated with the level of Cdk1 activity. To do so, we analyzed Polo signal in cells arrested in prometaphase with high Cdk1 activity as a result of colchicine treatment, which rapidly depolymerizes microtubules in mitotic neuroblasts (Fig. S3). We observed that the first phase of Polo association at lesions was similar in untreated and colchicine-treated cells (Fig. 1G,H). No significant difference in the half-time of Polo recruitment or its maximum levels at DNA lesions was observed between control and prometaphase-arrested cells (Fig. 1I,J). These results indicate that a functional spindle is not required for the efficient recruitment of Polo to DNA lesions. Interestingly, although Polo underwent a phase of dissociation from the lesions when untreated cells entered anaphase, Polo levels remained high and constant on the lesions in prometaphase-arrested cells (Fig. 1H). These results are consistent with a model in which Cdk1 activity is required for the maintenance of Polo at mitotic DSBs. Collectively, these results demonstrate the highly dynamic nature of Polo localization during mitosis, when it can be readily recruited to DNA lesions upon demand.

Inhibition of Polo kinase activity affects its kinetics at DNA lesions

The C terminus of Polo contains two Polo box domains (PBDs) that target Polo to different subcellular structures, such as centrosomes and unattached kinetochores, via recognition of phosphoepitopes that serve as docking sites to the PBDs (Elia et al., 2003a,b) (for review see Schmucker and Sumara, 2014). These phosphoepitopes on Polo targets are generated by priming kinases such as Cdk1, or by Polo itself (Kang et al., 2006; Lénárt et al., 2007). This prompted us to determine whether Polo kinase activity is required for its own recruitment to DNA lesions. To do so, we treated cells with BI2536, an inhibitor of Polo kinase activity (Lénárt et al., 2007; Riparbelli et al., 2014; Steegmaier et al., 2007). Polo inhibition is known to result in prolonged prometaphase (Conde et al., 2013; Lénárt et al., 2007; Llamazares et al., 1991; Sumara et al., 2004; Sunkel and
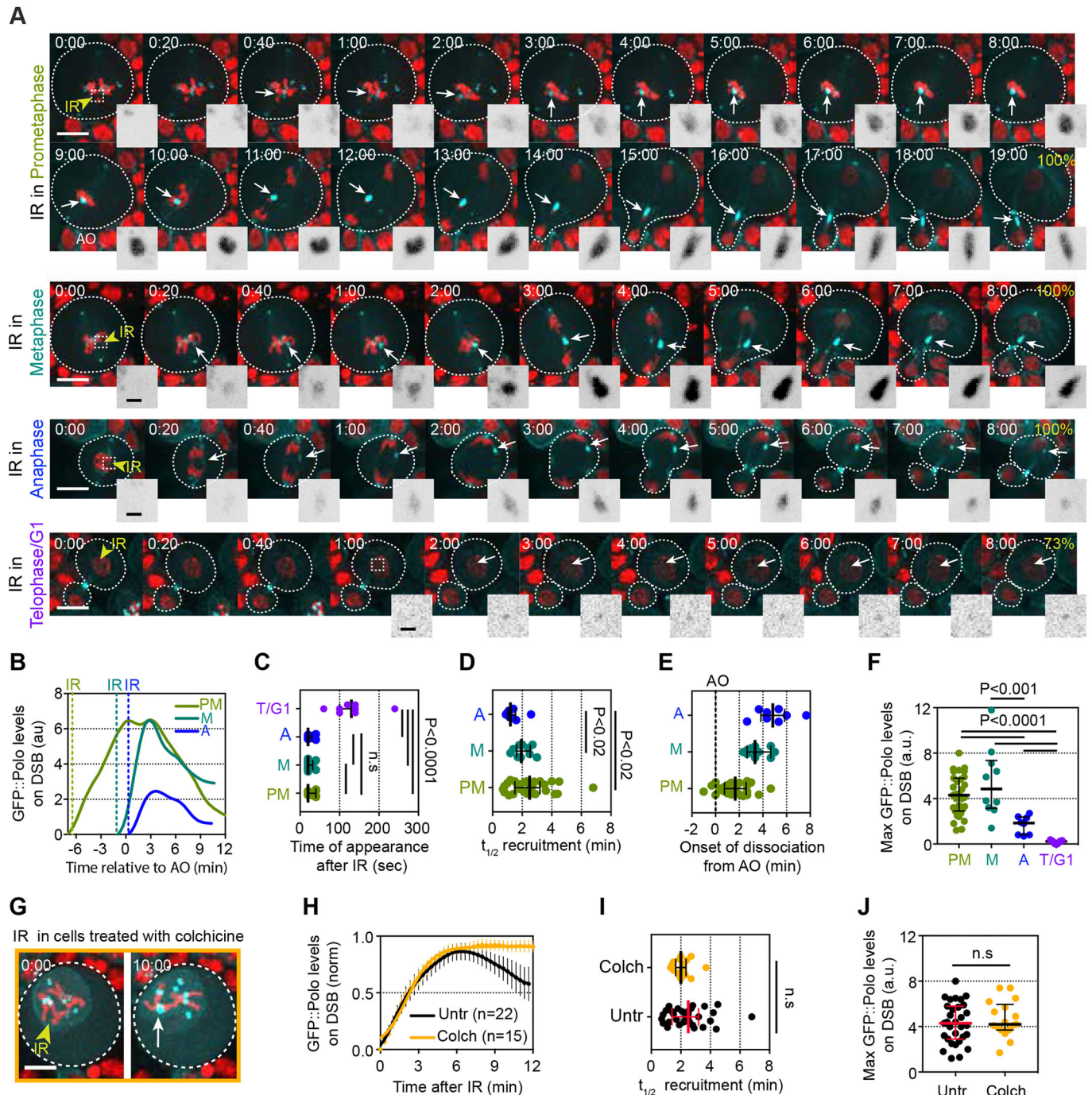
Fig. 1. Polo is recruited to laser-induced DNA breaks in mitosis and its maintenance at DNA lesions is coupled with Cdk1 activity. (A) Time-lapse images of *Drosophila* third instar larvae neuroblasts expressing H2A.Z::mRFP (red) and GFP::Polo (cyan) after IR of one chromosome during prometaphase (top rows), metaphase (second row), anaphase (third row) and telophase/G1 phase (bottom row). Images taken from Movies 1-3. Yellow arrowheads indicate the site of IR. Dashed squares represent the position of the insets. Time in min:s; 0:00 corresponds to the time of IR. White arrows point to the localization of the GFP::Polo signal at IR-induced DNA lesions. Insets show the inverted GFP::Polo signal at the site of IR. The percentage frequency of cells with a detectable GFP::Polo signal at the site of IR is indicated. (B) One example of GFP::Polo levels over time at DNA lesions induced after IR (dashed lines) during prometaphase (PM), metaphase (M) or anaphase (A). The time is relative to anaphase onset (t=0). (C-F) Scatter dot-plots showing the time of appearance (C), half-time of maximum recruitment ($t_{1/2}$) (D), onset of dissociation (E) and maximum levels (F) of GFP::Polo at the site of damage for the indicated conditions. (G) Time-lapse images of a neuroblast expressing H2Av::RFP (red) and GFP::Polo (cyan) arrested in prometaphase after 30 min treatment with colchicine (10 µM). Yellow arrowhead indicates the site of damage and the white arrow indicates the accumulation of GFP::Polo signal at the site of damage. (H) Average kinetics of GFP::Polo at DNA lesions in untreated cells (Untr; corresponding to cells in which the lesions were created in PM and monitored for more than 12 min) and in colchicine-treated cells (Colch). Dots and bars correspond to mean±95%CI. Yellow line corresponds to the data fit to a sigmoid equation $Y=\text{Max}/\{1+10^{[((t_{1/2})-X)\times\text{Hillslope}]}\}$ and the black line corresponds to the data smoothed with four averaged neighbors. n=number of cells. (I,J) Scatter dot-plots showing the half-time of recruitment ($t_{1/2}$) (I) and maximum levels (J) of GFP::Polo at the site of damage in untreated cells (Untr, corresponding to cells in which the lesions were created during PM) and cells treated with colchicine (Colch). Lines and bars correspond to median±interquartile range. Mann–Whitney two-tailed tests were used to calculate *P* values. Scale bars: 5 µm (images), 1 µm (insets).

Glover, 1988). Therefore, we compared GFP::Polo kinetics at DNA lesions in BI2536-treated cells with its kinetics in cells arrested in prometaphase after colchicine treatment, as colchicine did not affect the association phase of Polo at DSBs (as shown in Fig. 1H,I). We found that Polo inhibition using BI2536 severely altered GFP::Polo kinetics at DSBs (Fig. 2A,B). The initiation and the half-time of GFP::Polo recruitment to DNA lesions were delayed more than threefold upon BI2536 treatment (Fig. 2C,D). Similarly, BI2536-treated cells did not display the high levels of GFP::Polo on lesions observed in untreated cells or after colchicine treatment (Fig. 1J, Fig. 2E). Cells treated simultaneously with colchicine and BI2536 exhibited similar defects in Polo kinetics at DSBs to cells treated with BI2536 alone (Fig. 2A–D). Our results indicate that the rapid

and robust recruitment of Polo to DNA lesions depends on its kinase activity, as reported for its localization to centrosomes and kinetochores in human cells (Lénárt et al., 2007).

BubR1, Bub3 and Fzy display biphasic kinetics at DNA lesions during mitosis

Previously, we reported that BubR1 and Bub3 localized as a complex to damaged chromatids throughout mitosis, where they are required to sequester Fzy via its direct interaction with the KEN motif in BubR1 (Derive et al., 2015). We therefore analyzed the kinetics of GFP-tagged BubR1, Bub3 and Fzy after IR, as described for GFP::Polo. We observed that GFP::BubR1, GFP::Bub3 and GFP::Fzy were efficiently recruited to DNA breaks if the
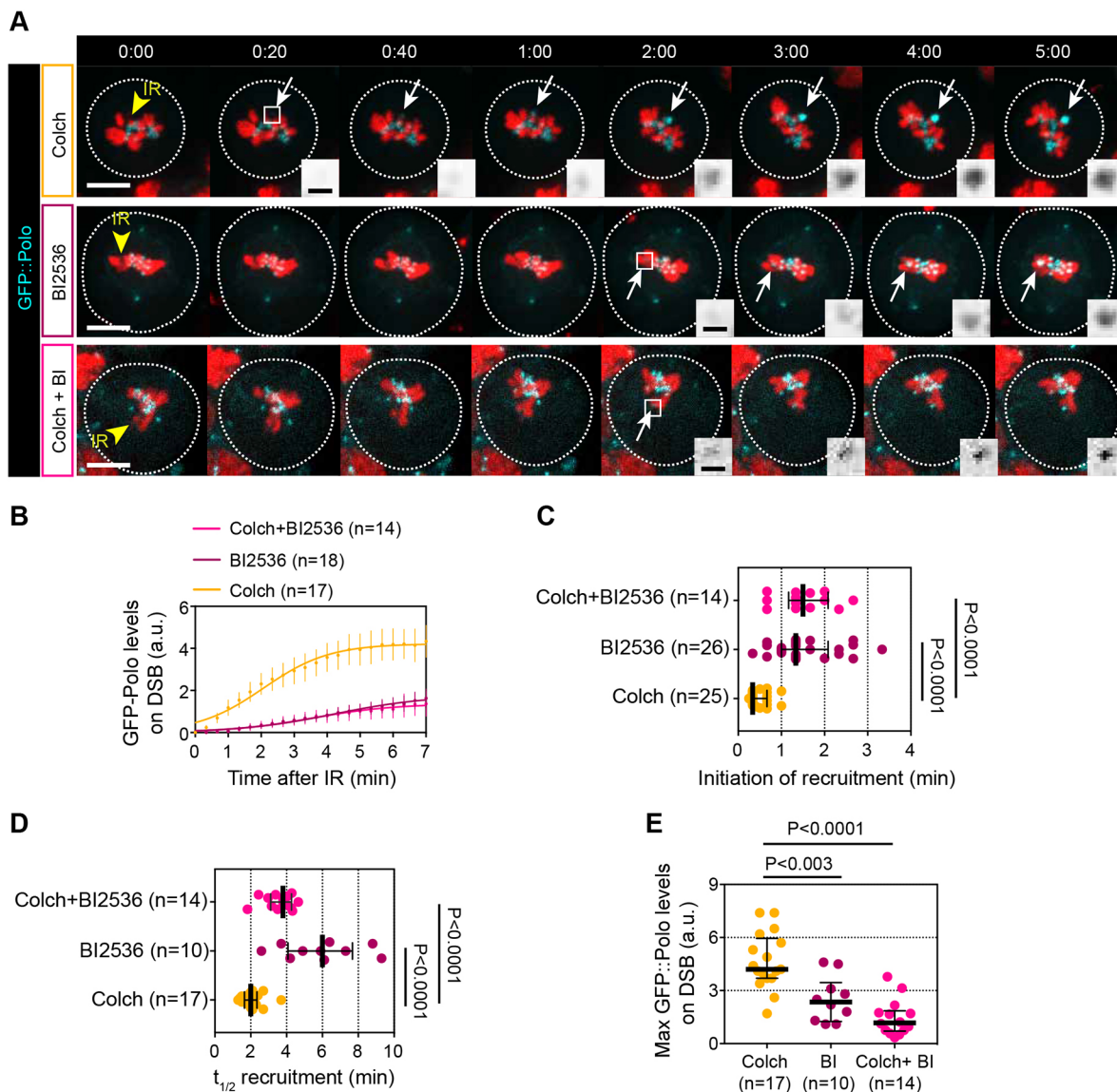
Fig. 2. Inhibition of Polo kinase activity with BI2536 alters Polo kinetics at DSBs in mitosis. (A) Time-lapse images of neuroblasts expressing H2A.Z::mRFP (red) and GFP:Polo (cyan) after IR (yellow arrowhead, t=0) previously treated with colchicine (top row), BI2536 (middle row) or both colchicine and BI2536 (bottom row) for 30 min. Images taken from Movie 4. White arrows indicate the localization of the proteins on DNA breaks. Insets show GFP::Polo inverted signal at the site of damage. Time in min:s. (B) Average kinetics of GFP::Polo at DNA lesions in cells pretreated with colchicine (Colch), BI2536 or both. Dots and bars represent mean±95%CI. Data were fit to the sigmoid equation $Y=\text{Max}/\{1+10^{[((t1/2)-X)\times \text{Hillslope}]}\}$. n=number of cells. (C) Scatter dot-plot showing the time when GFP::Polo is initially detected at laser-induced DNA lesions in cells pretreated with colchicine (Colch), BI2536 or both. (D) Scatter dot-plot displaying the half-time of recruitment ($t_{1/2}$) of GFP::Polo at the site of IR in cells treated with colchicine, BI2536 or both. (E) Scatter dot-plot displaying the maximum levels of GFP::Polo on DSBs in cells treated with colchicine (Colch), BI2536 (BI) or both. The lines correspond to median±interquartile range. A Mann–Whitney two-tailed test was used to calculate P values. Scale bars: 5 µm (images), 1 µm (insets).

damage occurred before anaphase (Fig. 3A). Their kinetics on DNA lesions was similar to GFP::Polo. All three proteins underwent a phase of association, culminating a few minutes after anaphase onset, followed by a phase of dissociation during anaphase/telophase (Fig. 3B,E). BubR1, Bub3 and Fzy shared similar timing of recruitment, which is consistent with their association to DSBs as a complex. However, their kinetics differed from Polo in three ways: First, their initiation and half-time of recruitment at the site of DNA damage were four and three times slower, respectively, compared with Polo (Fig. 3C,D). Second, unlike Polo, all three proteins dissociated completely from DBSs at telophase (Fig. 3B). Third, these proteins failed to localize to DNA lesions in more than half of the cells if the damage was induced after anaphase onset (Fig. 3A). This latter observation might be related to their slower rate of recruitment to DNA lesions, combined with their rapid and complete dissociation at telophase.

Polo precedes BubR1 on DNA lesions and a pool of Polo persists until interphase, whereas BubR1 completely dissociates from the lesions at telophase

The kinetics of Polo and the BubR1/Bub3/Fzy complex relative to each other at DSBs were monitored using simultaneous live-cell imaging of GFP::BubR1 and mCherry::Polo after IR (Fig. 4). In all instances, we observed that GFP::BubR1 foci appeared after mCherry::Polo at the site of damage (Fig. 4A-D). Consistently, the half-time of BubR1 recruitment was delayed compared with Polo (Fig. 4E). For both proteins, the phase of dissociation was initiated after anaphase onset (except in one cell for mCherry::Polo) (Fig. 4F). However, whereas BubR1 dissociation was complete at telophase, a pool of Polo remained on the lesions and disassembled at a later stage during the next interphase (Fig. 4G). Consequently, the half-time of Polo dissociation from damaged chromatids was slower than that of BubR1 (Fig. 4H). These simultaneous dual-color imaging data confirmed our previous observations on the rapid
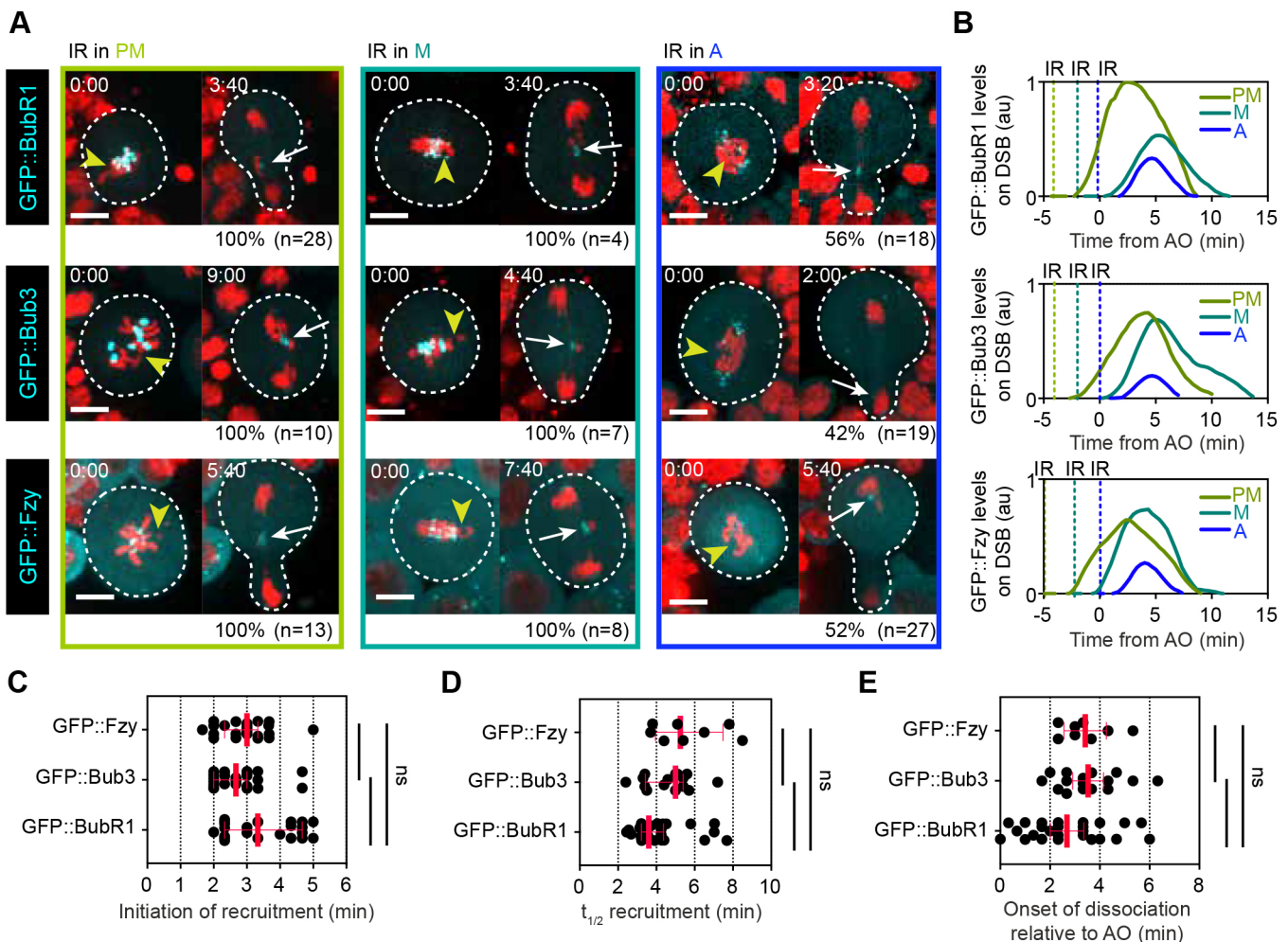
Fig. 3. BubR1, Bub3 and Fzy exhibit similar biphasic kinetics at DNA breaks in mitosis. (A) Time-lapse images of neuroblasts expressing H2A.Z::mRFP (red) and the indicated GFP-tagged proteins after IR was applied during prometaphase (PM), metaphase (M) or anaphase (A). Yellow arrowheads indicate the site of damage. White arrows indicate the localization of the proteins on DNA breaks. The frequency (%) of cells with a detectable signal of the indicated protein at DNA lesions as well as the total number of cells monitored (*n*) is specified under each panel. Time in min:s. (B) One example of kinetics of the indicated protein on DNA lesions depending on the stage of mitosis at which IR was applied (dashed line). Time 0 corresponds to anaphase onset. (C-E) Scatter dot-plots showing the time when the indicated protein was initially detected at DNA lesions (C), the half-time of recruitment ($t_{1/2}$) (D) and the onset of dissociation of the indicated proteins from the lesions (E). Red bars represent median±interquartile range. The three proteins display similar kinetics on DSBs, consistent with their localization as a complex. No significant difference between the kinetics of the three proteins was observed using a Mann–Whitney two-tailed test. Scale bars: 5 µm.
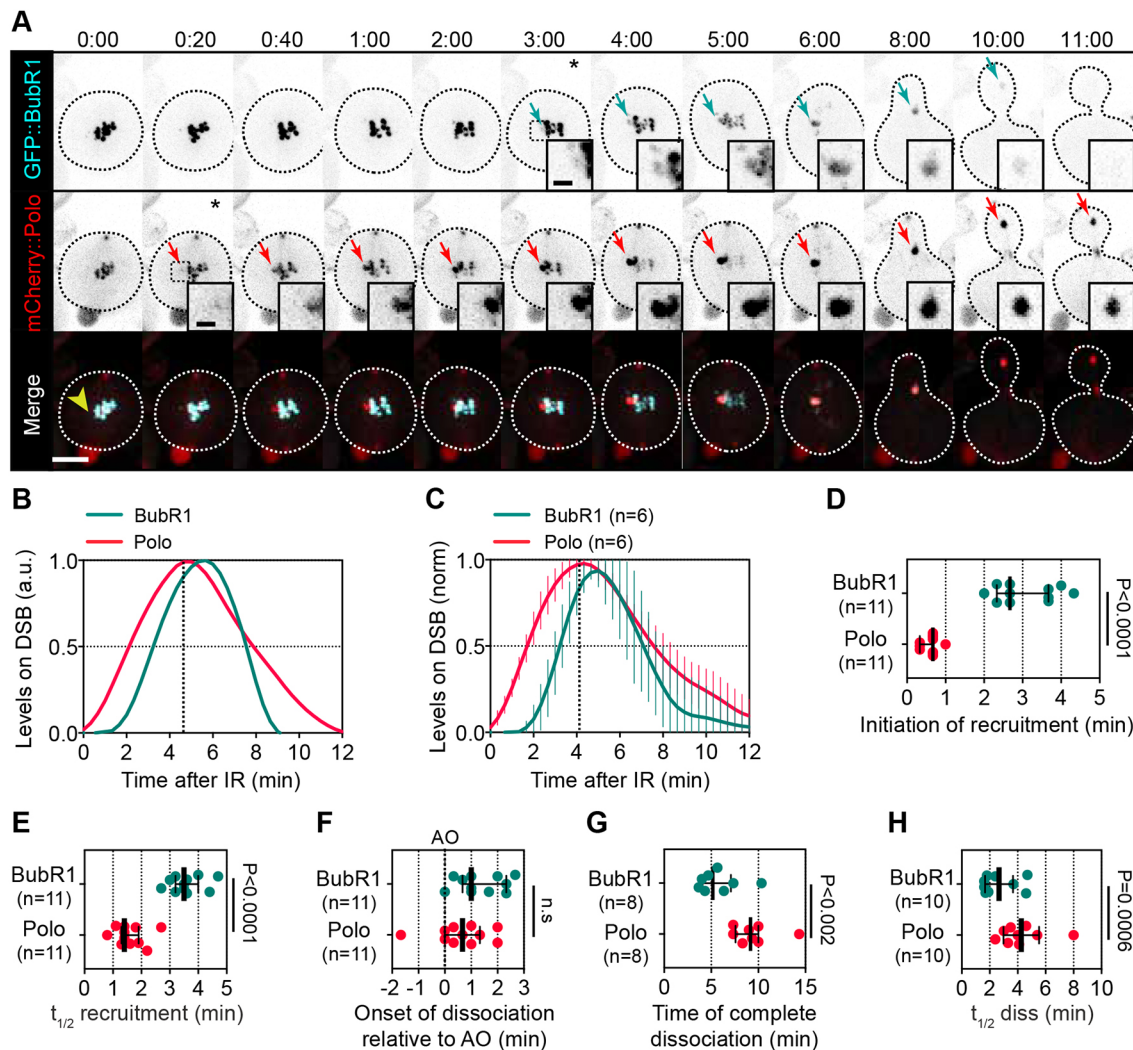
Fig. 4. BubR1 is recruited after Polo to DNA lesions and, unlike Polo, completely dissociates from the lesions at the end of mitosis. (A) Time-lapse images of neuroblasts expressing GFP::BubR1 (gray in top row and insets, cyan in bottom row) and mCherry::Polo (gray in middle row and insets, red in bottom row). Yellow arrowhead indicates the site of damage. Cyan and red arrows indicate the localization of GFP::BubR1 and mCherry::Polo on DNA breaks. Images taken from Movie 5. Insets in the top and middle rows are a magnification of the region of IR. Time in min:s. (B) Kinetics of the indicated proteins on DNA lesions in one cell. Data are normalized so that the maximum level for each protein equals 1. Lines correspond to the data smoothed with four averaged neighbors. Dashed line indicates the time of anaphase onset. Time 0 corresponds to the time of IR. (C) Average kinetics of mCherry::Polo and GFP::BubR1. Lines correspond to the data smoothed with four averaged neighbors. Bars indicate 95%CI. n=number of cells quantified. Dashed line represents the average time of anaphase onset. (D,E) Scatter dot-plots displaying the initiation (D) and half-time ($t_{1/2}$) (E) of recruitment of the indicated proteins to DNA lesions. (F-H) Scatter dot-plots displaying the onset (F), complete (G) and half-time of dissociation (H) of mCherry::Polo and GFP::BubR1 from the lesions after anaphase onset (AO). Bars represent median±interquartile range. A Mann–Whitney two-tailed test was used to calculate P values. Scale bars: 5 µm (images), 1 µm (insets).

association and slower dissociation kinetics of Polo at DNA breaks relative to BubR1.

Polo is required for the robust recruitment of BubR1 and Bub3 to DNA lesions during mitosis

The observation that Polo recruitment to DSBs precedes BubR1 and Bub3 prompted us to assess the requirement of Polo activity for the localization of BubR1 and Bub3 to sites of DNA damage. To do so, we monitored BubR1 and Bub3 dynamics in cells carrying a strong hypomorphic allele of *polo* (*polo[10]*) (Donaldson et al., 2001). Because attenuation of Polo activity induces a prolonged prometaphase (Conde et al., 2013; Llamazares et al., 1991; Sunkel and Glover, 1988), we compared the kinetics of BubR1 and Bub3 in *polo[10]* mutant cells with wild-type cells prolonged in prometaphase by colchicine treatment. Attenuation of Polo function severely altered the kinetics of BubR1 and Bub3 recruitment to

DNA lesions (Fig. 5A-C). The initiation and half-time of recruitment of both BubR1 and Bub3 to DNA breaks were greatly delayed compared with their kinetics in colchicine-induced prometaphase-arrested cells (Fig. 5D,E). To confirm this result, we monitored the kinetics of GFP::BubR1 in wild-type cells treated with the Polo inhibitor BI2536. Upon pharmacological inhibition of Polo activity, BubR1 signal was not detected at the site of DNA damage in the majority of cells (Fig. 5F). Collectively, these data indicate that Polo promotes the efficient recruitment of BubR1 and Bub3 to DNA breaks.

The DNA damage sensors Mre11 and Rad50 transiently associate with DSBs during mitosis

In a previous study, we reported that none of the core kinetochore proteins (including CenpA/Cid, CenpC, Spc105, Spc25 and Nuf2) nor members of the spindle assembly checkpoint (Mps1, Mad1,
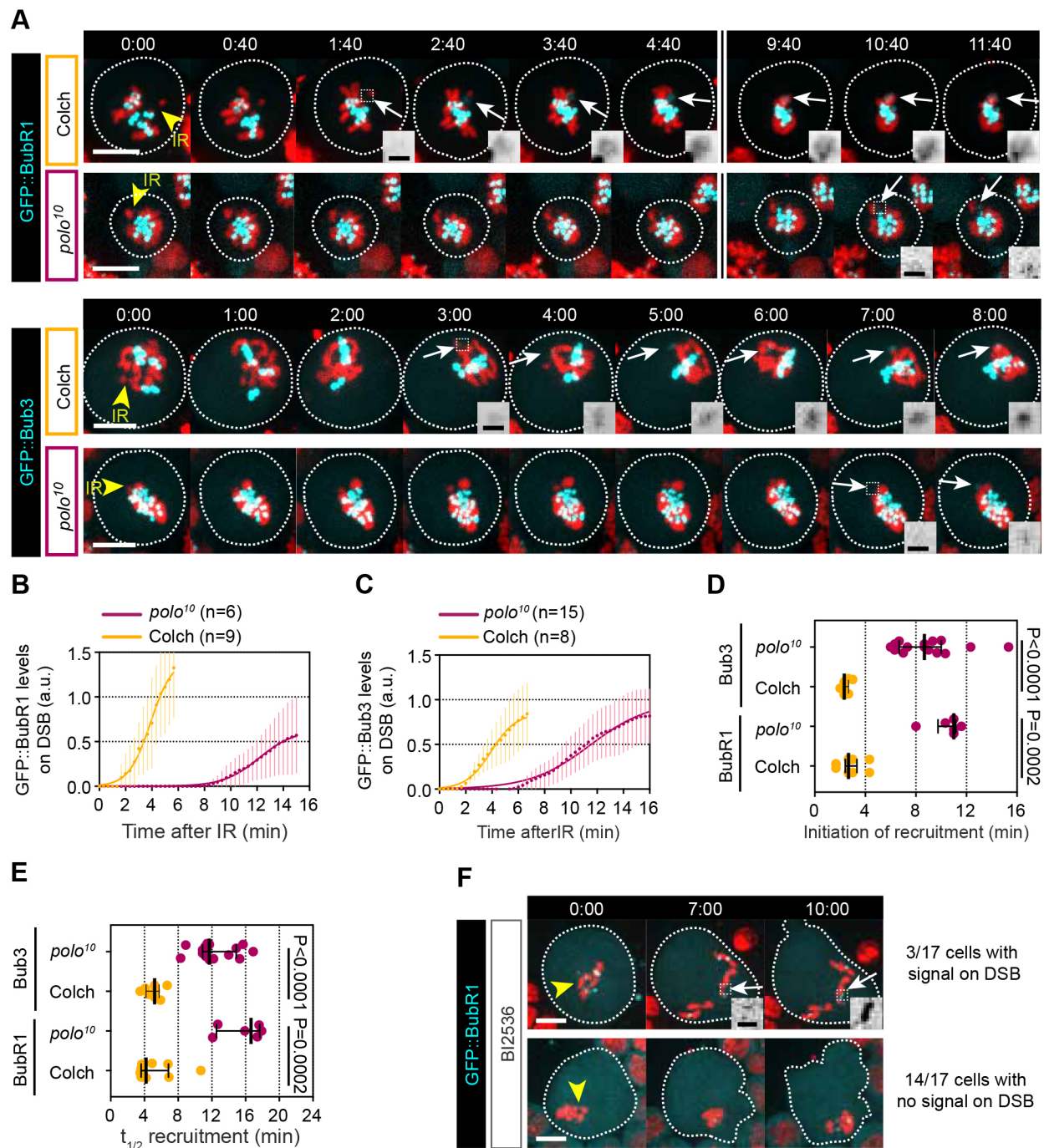
Fig. 5. Attenuation of Polo activity affects BubR1 and Bub3 kinetics at DNA lesions in mitosis. (A) Time-lapse images of neuroblasts expressing H2A.Z::mRFP (red) and GFP::BubR1 (cyan in top row, gray in insets) or GFP::Bub3 (cyan in bottom row and gray in insets) after IR (yellow arrowheads, time=0). The kinetics of GFP::BubR1 and GFP::Bub3 at DNA lesions were compared between wild-type cells arrested in prometaphase after colchicine treatment (Colch) and $polo^{10}$ mutant cells. Images taken from Movies 6 and 7. White arrows indicate the localization of the proteins on DNA breaks. Dashed squares represent the inset regions. (B,C) Kinetics of GFP::BubR1 (B) and GFP::Bub3 (C) at DSBs after IR (t=0). Dots and bars correspond to mean±95%CI. Data were fit to the sigmoid function $Y=\text{Max}/\{1+10^{[((t1/2)-X)\times\text{Hillslope}]}\}$. (D,E) Scatter dot-plot showing the initiation (D) and half-time ($t_{1/2}$) (E) of recruitment of the indicated proteins to DSBs in colchicine-treated wild-type cells and $polo^{10}$ mutant cells. Bars correspond to median±interquartile range. A Mann–Whitney two-tailed test was used to calculate P values. (F) Time-lapse images of neuroblasts expressing GFP::BubR1 (cyan and insets) and H2A.Z::mRFP (red) treated with the Polo inhibitor BI2536 after IR (yellow arrowhead, t=0). Top row shows 1 of 3 out of 17 BI2536-treated cells in which GFP::BubR1 signal was detected on DSBs (white arrow, insets). Bottom row displays one of 14 out of 17 BI2536-treated cells in which no GFP::BubR1 signal was detected on DSBs. Dashed square represents the inset region. Time in min:s. A Mann–Whitney two-tailed test was used to calculate P values. Scale bars: 5 µm (images), 1 µm (insets).

Mad2) localized on I-CreI- or laser-induced DSBs (Derive et al., 2015; Royou et al., 2010). These data suggest that the formation of a neo-kinetochore on broken chromosomes is highly unlikely. As Cid is required for the localization of Polo and BubR1 on kinetochores (Blower and Karpen, 2001), we reasoned that Polo and BubR1/Bub3 localization on DNA breaks is likely to be mediated via interactions with components that do not depend on kinetochore proteins. Recent studies in vertebrates reported that components of

the early steps of the DDR, including the MRN complex, ATM and γH2AX, form foci on damaged chromosomes during mitosis (Giunta et al., 2010; Gomez-Godinez et al., 2010; Orthwein et al., 2014). Similarly, γH2A.Z foci were detected on damaged chromatids in *Drosophila* neuroblasts (Royou et al., 2010), suggesting that activation of the initial steps of the DDR in mitosis is conserved in *Drosophila*. It therefore seemed possible that activation of the first steps of the DDR during mitosis promotes the recruitment of Polo and, consequently, BubR1 and Bub3 to DNA lesions.

Thus, we examined the dynamics of the DSB sensors Mre11 and Rad50 on sites of laser-induced DNA damage in mitotic neuroblasts. One dose of mRFP-Rad50 rescued the lethality associated with a *rad50EP* strong hypomorph mutation, demonstrating that mRFP did not ablate Rad50 function. Next, the dynamics of GFP::Mre11 and mRFP::Rad50 were monitored on DNA lesions at different stages of mitosis. Mre11 and Rad50 signals appeared within 5-10 s of IR, which was even more rapid than the Polo signal (Fig. 6A). As was the case for Polo, BubR1 and Bub3, both Mre11 and Rad50 exhibited biphasic kinetics at DNA lesions, with a phase of association promptly followed by a phase of dissociation (Fig. 6A,B). We also observed the re-association of Mre11 and Rad50 at sites of DNA damage, coupled with their nuclear localization upon entry into the next interphase (Fig. 6A, last insets). Remarkably, the biphasic kinetics of Mre11 and Rad50 did not correlate with the timing of anaphase onset (Fig. 6B), in contrast to the kinetics of Polo, BubR1, Bub3 and Fzy. Consequently, the half-time of Mre11 recruitment was less than 1 min, regardless of the stage of mitosis at which DSBs were induced (Fig. 6C,D). These observations suggest that the level of Cdk1 activity has minimal effect on MRN kinetics at DSBs. However, when IR was applied during anaphase, Mre11 did not reach the same levels on DSBs as observed during other points in mitosis (Fig. 6E). This puzzling observation led us to test the influence of Cdk1 activity on Mre11 dynamics at lesions by monitoring GFP:: Mre11 in colchicine-treated, prometaphase-arrested cells after IR. No difference in Mre11 kinetics was detected between cells going through mitosis and prometaphase-arrested cells (Fig. 6C-E). This result suggests that, unlike Polo, high Cdk1 activity does not prevent Mre11 dissociation from DSBs.

Next, we examined the differences in kinetics between the MRN complex and Polo on mitotic DNA lesions by dual-color imaging of neuroblasts expressing both GFP::Mre11 and mCherry::Polo (Fig. 6F,G). As previously observed, GFP::Mre11 signal promptly appeared at the site of IR, preceding mCherry::Polo (Fig. 6F-H). GFP::Mre11 recruitment to DSBs was brief and invariably initiated its dissociation in less than 3 min after IR, regardless of the stage of mitosis (Fig. 6F,G). In contrast, mCherry::Polo consistently remained associated at the damaged chromosome until anaphase onset (Fig. 6E,G,I). This point is illustrated by the observation that its half-time of recruitment has a greater variance than that of GFP:: Mre11 (Fig. 6H).

Depletion of MRN affects Polo kinetics at DNA lesions

Because Mre11 precedes Polo at the site of IR, we hypothesized that the recognition of DSBs by the MRN complex during mitosis facilitates the recruitment of Polo and, subsequently, BubR1 and Bub3 to DNA breaks. To test this idea, we monitored the dynamics of Polo in *rad50* mutant cells. Rad50 is an essential protein in *Drosophila*, and null or strong hypomorphic alleles result in lethality at the pupal stage (Ciapponi et al., 2004; Gorski et al., 2004). Furthermore, Rad50 as well as Mre11 and Nbs1 have conserved functions in DNA repair signaling and telomere

protection (Ciapponi et al., 2004, 2006; Gorski et al., 2004; Sekelsky, 2017).

We first confirmed that Mre11 was no longer detected on DSBs in mitosis in *rad50EP* strong-hypomorph mutant cells (Fig. 7A). Then, we monitored the kinetics of recruitment of GFP::Polo in *rad50EP* mutant cells after IR (Fig. 7B,C). We observed that attenuation of Rad50 severely altered Polo dynamics at DSBs. The time of Polo appearance at DNA lesions and its half-time of recruitment were both greatly delayed (Fig. 7D,E). Similarly, Polo did not reach the high levels at DNA lesions observed in wild-type cells in *rad50EP* mutant cells (Fig. 7F). These results indicate that the MRN complex acts upstream of Polo at mitotic DSBs.

Stable localization of Mre11 to chromatin is sufficient to recruit Polo independently of DNA damage

Previous studies demonstrated that prolonged binding of the MRN complex to chromatin was sufficient to trigger the recruitment and activation of downstream components of the DDR independently of DNA damage (Bonilla et al., 2008; Soutoglou and Misteli, 2008). To determine whether ectopic localization of the MRN complex to chromatin was sufficient to recruit Polo independently of DNA lesions in mitosis, we fused Mre11 to the *Escherichia coli* lactose repressor (LacI), tagged with GFP. The construct was introduced into flies carrying an X chromosome with 256 repeats of the lac operator sequence (LacO) located near the telomere (Fig. 8A) (Belmont and Straight, 1998). We first checked that the fusion protein was efficiently recruited to laser-induced DNA damage during mitosis, and that it co-localized with mRFP::Rad50 and mCherry::Polo at the site of damage (Fig. S4A,B). Next, we monitored the localization of the fusion proteins in flies carrying one X chromosome with 256 LacO repeats. As expected, GFP:: LacI::Mre11 signal was observed as distinct foci on LacO arrays in 73% of mitotic cells (Fig. 8B). We did not observe any obvious defects in chromatid segregation, suggesting that the persistent tethering of Mre11 to chromatin did not affect genome integrity. In the seven mitotic cells where GFP::LacI::Mre11 was detected on LacO arrays, three cells exhibited mRFP::Rad50 foci colocalizing transiently with GFP::LacI::Mre11. This result indicates that the ectopic localization of Mre11 on chromatin resulted in the recruitment of Rad50, as demonstrated in human cells (Fig. 8B) (Bonilla et al., 2008; Soutoglou and Misteli, 2008). Remarkably, mCherry::Polo signal was also detected with GFP::LacI::Mre11 foci in 25% of cells (Fig. 8B). This result indicates that the tethering of Mre11 to chromatin is sufficient to recruit Polo independently of DNA damage.

The DNA repair component Okra does not localize on mitotic DSBs

In vertebrates, the pathway downstream of MRN and ATM involved in DNA repair by NHEJ or HR is inhibited during mitosis (Giunta et al., 2010; Orthwein et al., 2014; Peterson et al., 2011; Terasawa et al., 2014). To determine whether this inhibition is conserved in *Drosophila* after IR, we monitored the dynamics of Okra (*Drosophila* homolog of human RAD54), a helicase involved in DNA repair by HR (Kooistra et al., 1999; Schupbach and Wieschaus, 1991; Sekelsky, 2017). As expected, a prominent Okra::GFP focus was detected at the site of laser-induced damage in interphase nuclei, indicating that DNA repair by HR was initiated (Fig. S5, cell#2). In contrast, no Okra::GFP signal was observed on damaged chromosomes in mitotic cells (Fig. S5, cell#1). Collectively, theses results provide evidence that, similar to vertebrates, the early steps of the DDR are activated upon DNA
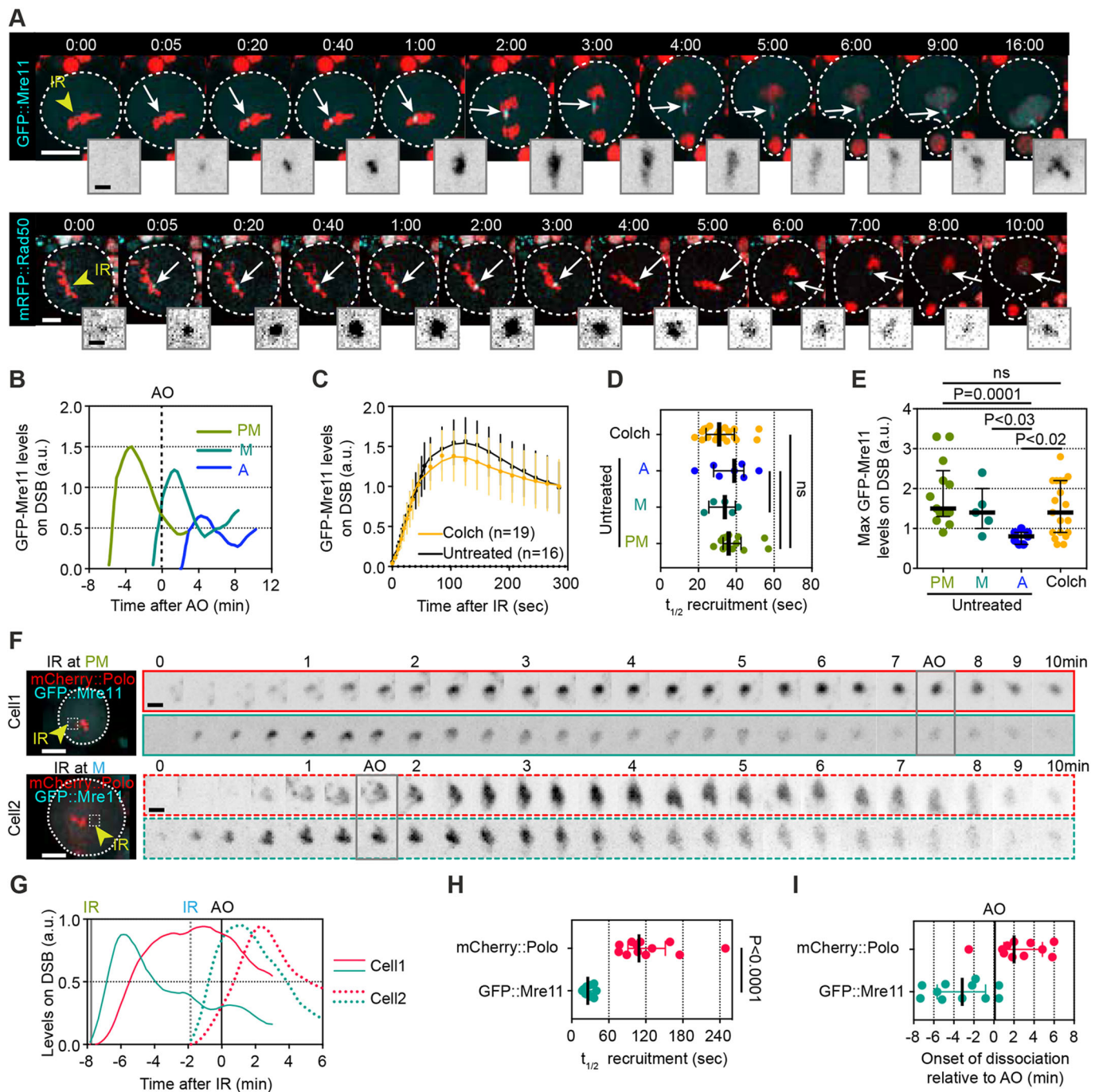
Fig. 6. Mre11 and Rad50 precede Polo on IR-induced DSBs but, unlike Polo, dissociate rapidly from the lesions regardless of the stage of mitosis.
(A) Time-lapse images of neuroblasts expressing H2A.Z::mRFP (red) and GFP::Mre11 (top row, cyan and insets) or H2A.Z::GFP (red) and mRFP::Rad50 (bottom row, cyan and insets) after IR (yellow arrowhead, t=0). White arrows highlight the localization of the indicated proteins on DNA lesions. Time in min:s. (B) Representative kinetics of GFP::Mre11 at DNA lesions after IR was applied during prometaphase (PM), metaphase (M) or anaphase (A). Time 0 corresponds to anaphase onset (AO). (C) Kinetics of GFP::Mre11 at DNA lesions after IR in untreated cells (untr; IR was applied during prometaphase) or cells previously treated with colchicine (Colch). Dots and bars represent mean±95%CI. Lines correspond to the data smoothed with four averaged neighbors. (D,E) Scatter dot-plots showing the half-time of recruitment ($t_{1/2}$) (D) and the maximum levels (E) of GFP:: Mre11 for the indicated conditions. Time 0 corresponds to the time of IR. Bars correspond to median±interquartile range. (F) Images of neuroblasts co-expressing mCherry::Polo (red) and GFP::Mre11 (Cyan). IR was applied at prometaphase (cell 1, top row) and metaphase (cell 2, bottom row). Yellow arrowheads point to the site of IR. Insets correspond to the inverted mCherry::Polo (top row) and GFP::Mre11 (bottom row) channels at the site of IR (delineated by a dashed square in the first images). Frames corresponding to the time of anaphase onset are highlighted with a gray square for each cell. (G) Graphs showing the corresponding kinetics of GFP::Mre11 and mCherry::Polo at DNA lesions for cell 1 (solid line) and cell 2 (dashed line) shown in A. (H,I) Scatter dot-plots showing the half-time of recruitment ($t_{1/2}$) (H) and onset of dissociation (I) of GFP::Mre11 and mCherry::Polo from the DNA lesions. Bars correspond to median±interquartile range. A Mann–Whitney two-tailed test was used to calculate P values. Scale bars: 5 µm (images), 1 µm (insets).
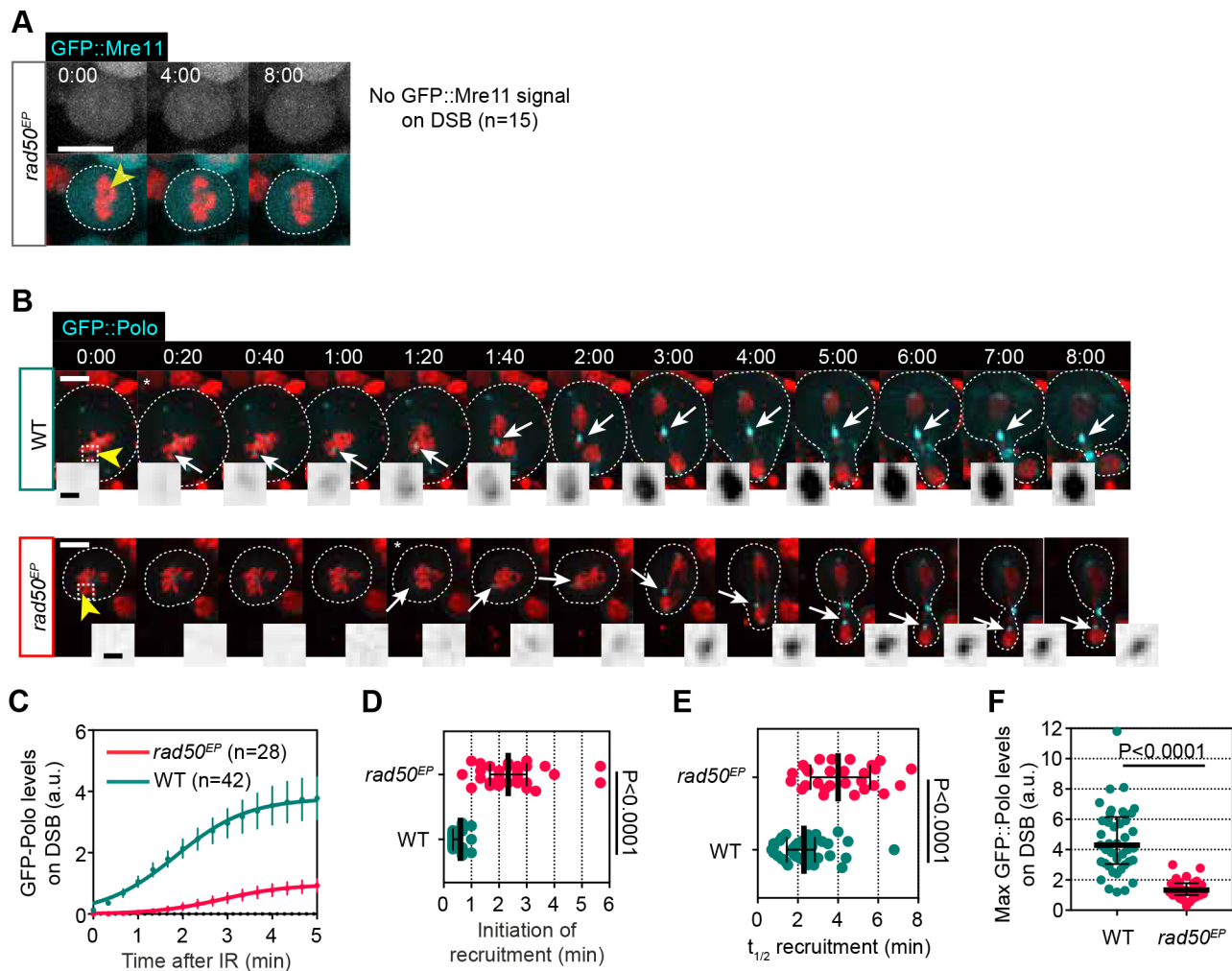
Fig. 7. The robust recruitment of Polo to DNA breaks in mitosis depends on Rad50. (A) Time-lapse images of *rad50^EP* mutant neuroblasts expressing H2A.Z::mRFP (red) and GFP::Mre11 (gray in top row and cyan in bottom merged images) after IR (yellow arrowhead, *t*=0). No GFP::Mre11 signal is detected on DNA breaks in 100% of *rad50^EP* mutant cells (*n*=15). Dashed lines delineate the cell. Time in min:s. (B) Time-lapse images of wild-type (WT, top row) and *rad50^EP* mutant (bottom row) neuroblasts expressing H2Az::mRFP (red) and GFP::Polo (cyan and insets) after IR (yellow arrowheads, *t*=0). Images taken from Movie 10. White arrows show the localization of GFP::Polo at the site of damage. Asterisk indicates the time of appearance of GFP::Polo on DSBs. Insets correspond to the GFP::Polo level at the site of damage (dashed squares on the first images). Dashed lines delineate the cells. (C) Average kinetics of GFP::Polo at the site of damage in wild-type and *rad50^EP* mutant cells after IR. Dots and bars correspond to mean±95% c.i. Data are fit to the sigmoid equation $Y=\text{Max}/\{1+10^{[((t1/2)-X)\times\text{Hillslope}]}\}$. (D-F) Scatter dot-plots showing the initiation (D), half-time (*$t_{1/2}$*) of recruitment (E) and maximum level of GFP::Polo at the site of damage for the indicated genotype. Lines and bars correspond to median±interquartile range. A Mann–Whitney two-tailed test was used to calculate *P* values. Scale bars: 5 µm (images), 1 µm (insets).

damage in *Drosophila* mitotic cells. This is followed by inhibition of the Okra-dependent downstream repair pathway.

DISCUSSION

Using live single-cell analysis combined with surgical damage of one chromosome at a defined time during mitosis, we have performed detailed analysis of the kinetics of the mitotic proteins Polo, BubR1, Bub3 and Fzy and the DSB sensors Mre11 and Rad50 on mitotic DSBs. Our studies show that Mre11 and Rad50 transiently associate with DSBs and facilitate the robust recruitment of Polo and, consequently, the BubR1/Bub3 complex to DSBs. This, combined with our previous observation that Polo, BubR1 and Bub3 are required for tethering of the two broken chromosome ends, can be integrated within the following model: DSBs in mitosis are promptly marked by the MRN complex, promoting the recruitment of Polo kinase (Fig. 8C). Subsequently, the MRN complex dissociates from DSBs, possibly to prevent

activation of downstream repair components, while Polo kinase activity promotes the subsequent accumulation of the BubR1/Bub3 complex at DSBs. This complex sequesters Fzy, thereby inhibiting the APC/C locally. Polo and BubR1/Bub3 levels are maintained at DSBs until mid-anaphase, thus facilitating the persistent tethering of broken fragments at a crucial time during poleward chromosome movement. Upon segregation of the broken DNA fragment, Polo and the BubR1/Bub3/Fzy complex dissociate from the DNA lesions. However, a pool of Polo persists on DSBs through the next interphase, while MRN re-accumulates at the site of damage to promote downstream repair signaling (Fig. 8C) (Derive et al., 2015; Royou et al., 2010).

Polo kinetics at mitotic DSBs

We observed that Polo promptly accumulates at DSBs at any point during mitosis, including anaphase, albeit with lower levels. The kinetics of its recruitment are sigmoidal, suggesting the cooperative
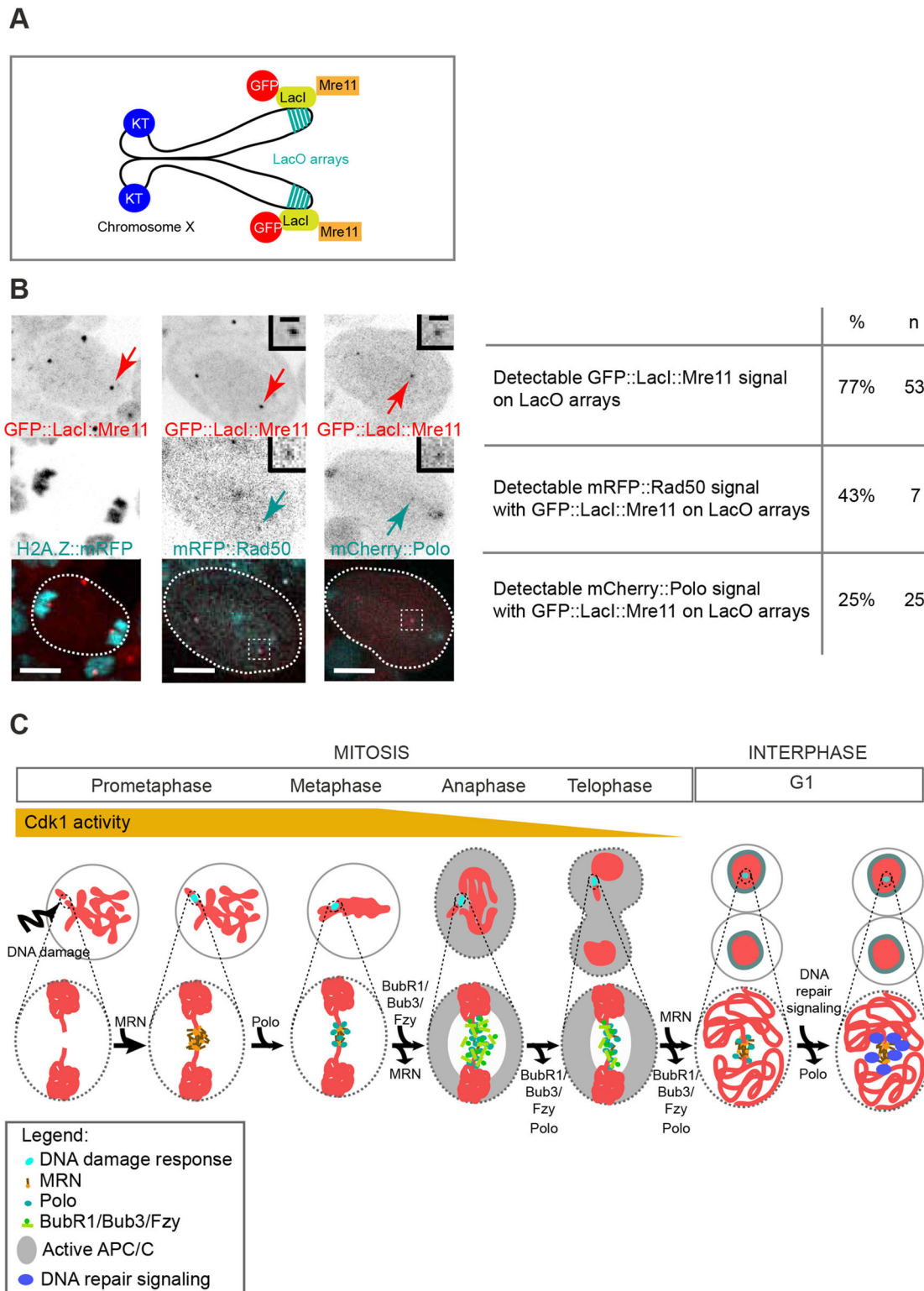
Fig. 8. Ectopic localization of Mre11 on chromatin is sufficient to recruit Polo independently of DNA damage. (A) Scheme of *Drosophila* chromosome X containing 256 LacO repeats located at position 1E. These repeats are binding sites for the *E. coli* transcriptional repressor LacI. The expression of GFP::LacI fused to Mre11 suffices to target Mre11 to the LacO repeats. (B) Still images from time-lapse movies of neuroblasts expressing GFP::LacI::Mre11 (top row and insets, red in merge) and H2A.Z::mRFP, mRFP::Rad50 or mCherry::Polo (middle row and insets, cyan in merge). Time in min:s. Red arrows indicate the GFP::LacI::Mre11 LacO arrays. Table shows the corresponding percentage of cells positive for GFP::LacI::Mre11 signal on LacO arrays and percentage of cells with mRFP::Rad50 or mCherry::Polo signals colocalizing with GFP::LacI::Mre11 on LacO arrays. *n*=number of cells. (C) Model for the DNA damage response in mitosis. After DNA damage, the MRN complex is promptly but transiently recruited to DSBs and targets Polo to the site of damage. Polo subsequently promotes the recruitment of the BubR1/Bub3 complex, which sequesters Fzy and inhibits the APC/C at the site of DNA damage during poleward movement of sister chromatids. BubR1/Bub3 dissociate from the DSBs at telophase, while a pool of Polo remains associated with DSBs into the next interphase. Meanwhile, MRN re-accumulates on DSBs, promoting the activation of downstream repair components. Scale bars: 5 µm (images), 1 µm (insets).

binding of Polo at the site of damage. Given that Polo localization to subcellular structures is mediated through its interaction with primed phosphorylated substrates (Elia et al., 2003a,b; Schmucker and Sumara, 2014), our findings that pharmacological inhibition of Polo kinase activity severely alters Polo recruitment to DSBs, but does not completely prevent it, supports the conclusion that Polo kinase activity is not required for the initial steps of DSB association but promotes its cooperative binding to DSBs through a self-priming mechanism. Interestingly, recent studies have reported that MRE11 is a substrate of polo-like kinase 1 (PLK1) in human cells (Li et al., 2017; Xu et al., 2018). It is therefore conceivable that Polo promotes its recruitment to DSBs via phosphorylation-dependent priming of Mre11.

Several lines of evidence suggest that Cdk1 activity modulates Polo kinetics at DSBs. First, Polo initiates its dissociation from DSBs invariably during anaphase, in concert with the decline of Cdk1 activity. Second, Polo levels are constantly maintained at DSBs in prolonged prometaphase when Cdk1 activity is high. Finally, Polo never reaches the high levels on DSBs created during anaphase. Although the molecular mechanism by which Cdk1 contributes to Polo kinetics at DSBs remains to be elucidated, we can propose plausible possibilities. Numerous Polo substrates are primed by Cdk1 (Lowery et al., 2005); thus, Cdk1 may facilitate the enrichment of Polo at DNA lesions by priming Polo targets associated with DSBs. Alternatively, Cdk1 may sustain Polo activation at DSBs directly through phosphorylation of the T-loop in the kinase domain (Mortensen et al., 2005), or indirectly by inhibiting counteracting phosphatases. The observation that Polo is successfully recruited to DSBs induced at anaphase, albeit with less efficiency, suggests that Cdk1 activity is not essential for the initial steps of Polo recruitment to DSBs but is important for its cooperative binding and maintenance at the lesions.

Polo promotes the robust recruitment of BubR1/Bub3 to mitotic DSBs
In this study, we demonstrate that one of the functions of Polo at mitotic DSBs is to target the BubR1/Bub3 complex. Polo precedes BubR1/Bub3 on DSBs and attenuation of its kinase activity dramatically alters the kinetics of BubR1/Bub3 at DSBs. This raises the question of how Polo mediates the recruitment of BubR1/Bub3 to DSBs. One possibility is via direct phosphorylation of BubR1 by Polo. In a previous study, we found that a 432 amino acid fragment of BubR1 (from amino acid 330 to amino acid 762) was sufficient for its localization to mitotic DSBs. This sequence encompasses a conserved motif called KARD, which is phosphorylated by PLK1 in human cells, resulting in the interaction of BubR1 with the phosphatase PP2A-B56α at kinetochores (Espert et al., 2014; Kruse et al., 2013; Suijkerbuijk et al., 2012). However, it is unlikely that Polo mediates the localization of BubR1/Bub3 to DSBs via direct phosphorylation of the BubR1 KARD motif, because mutation of the putative Polo phosphosites to alanine or aspartate had no obvious effect on the localization of BubR1 to mitotic DSBs (Derive et al., 2015). However, this 432 amino acid sequence includes seven other Polo putative phosphosites, including serine at position 581, which is phosphorylated *in vivo* in *Drosophila* embryos (Zhai et al., 2008). It would be relevant to determine whether any of these putative Polo phosphosites are important for BubR1 targeting to DSBs. Alternatively, Polo might target BubR1/Bub3 to DSBs indirectly by promoting interactions with another substrate. Studies have shown that Bub3 is targeted to the kinetochore via direct interaction with the kinetochore scaffold KNL1. This interaction involves the recognition of phosphorylated

MELT repeats in KNL1 by two residues in Bub3 (Primorac et al., 2013). Importantly, although the MELT repeats are phosphorylated primarily by the spindle checkpoint component Mps1, studies have shown that Plk1 also contributes to this phosphorylation (Espeut et al., 2015). Interestingly, sequence analysis reveals that *Drosophila* Rad50 contains two MELT repeats. In addition, the residues identified in human BUB3 that are crucial for its interaction with the phosphorylated MELTs are conserved in *Drosophila* Bub3. Although speculative, it is possible that Polo phosphorylates Rad50 on its MELT repeats at mitotic DSBs, and these phospho-MELTs, in turn, target the BubR1/Bub3 complex via direct interaction with Bub3. It would be relevant to determine the importance of the conserved Bub3 residues and the Rad50 MELT repeats in the recruitment of BubR1/Bub3 to DSBs.

MRN associates transiently to mitotic DSBs
Although the detection of DSBs in interphase can be facilitated by confinement of the DSBs sensors in the nucleus and their association to chromatin, the recognition of DSBs during mitosis poses a greater challenge, as the DSBs sensors are dispersed throughout the cytoplasm (Polo and Jackson, 2011). Here, we show that cytoplasmic Mre11 and Rad50 readily accumulate on DSBs in mitosis with a half-time of recruitment estimated at around 30-40 s, modestly faster than that observed for human RAD50 on interphase DSBs using the same method of IR ($t_{1/2}$~60 s) (Aleksandrov et al., 2018). This result is consistent with the detection of mitotic and interphase DSBs by MRN via a conserved mechanism. Experiments using single molecule tracking of MRN on *in vitro* reconstituted DNA homoduplexes have provided evidence that chromatin-associated MRN detects free DNA ends by scanning the DNA molecule through facilitated diffusion (Myler et al., 2017). However, as MRN is excluded from the condensed chromosomes, this chromatin-dependent diffusion-based mechanism is unlikely to occur on mitotic DSBs. It is possible that the initial detection of free DNA ends occurs through a different pathway, possibly through cytoplasmic diffusion but, once associated, a minimal amount of MRN triggers the rapid and robust accumulation of additional MRN molecules via cooperative binding, as suggested by the sigmoidal shape of Mre11 recruitment to mitotic DSBs. We cannot rule out that an undetected pool of MRN complex remains associated to condensed chromatin during mitosis and senses DSBs through active diffusion, as demonstrated *in vitro* (Myler et al., 2017).

The recruitment of Mre11 and Rad50 to mitotic DSBs is strikingly transient. Maximum levels are observed ~2 min following laser IR and they subsequently dissociate rapidly from DSBs ($t_{1/2}$ dissociation ~2 min), until the next interphase when they re-accumulate on the lesions. Although the kinetics of *Drosophila* MRN at DSBs during interphase is not known, our result contrasts with observations of human RAD50 in the interphase nucleus, where its removal from DSBs is slow ($t_{1/2}$>30 min) (Aleksandrov et al., 2018). We currently do not know the biological significance of the prompt dissociation of Rad50 and Mre11 from mitotic DSBs and how it is controlled. One possibility is that the transient association of MRN with mitotic DSBs is sufficient to initiate the recruitment of Polo and, consequently, BubR1/Bub3, but its ensuing rapid dissociation prevents the unscheduled recruitment of downstream DNA repair components to damage chromatin, which could otherwise compromise sister chromatid segregation. This idea is consistent with the observations that DNA repair signaling downstream of MRN is inhibited during mitosis (Giunta et al., 2010; Orthwein et al., 2014; Peterson et al., 2011; Terasawa

12

et al., 2014) (this study) and that its reactivation provokes telomere fusion (Orthwein et al., 2014). If this model is correct, one might expect to observe an alteration of chromosome structure that would lead to segregation defects upon prolonged association of MRN with mitotic DSBs. However, no noticeable defects in chromosome segregation were observed in cells where Mre11 was persistently tethered to X chromosome-associated LacO arrays. These results should be interpreted cautiously because mRFP::Rad50 colocalized with LacO-associated GFP::LacI-Mre11 foci in less than half of the cells observed and most of the GFP::LacI::Mre11 and mRFP::Rad50 signal was associated with large cytoplasmic aggregates. Therefore, the amount of functional MRN complex generated using this approach might be insufficient to induce a dominant negative effect. The future challenge is to decipher the underlying mechanisms that control MRN kinetics on mitotic DSBs.

MRN promotes the robust recruitment of Polo to mitotic DSBs

We found that depletion of MRN severely alters Polo kinetics at mitotic DSBs. Conversely, ectopic targeting of Mre11 to chromosomes is sufficient to recruit Polo, albeit with low efficiency. Collectively, these data strongly argue that the MRN complex plays a positive role in targeting Polo to DSBs. As discussed above, MRN might promote Polo association with DSBs via direct interaction with Mre11. Alternatively, MRN might target Polo to DSBs indirectly through the recruitment of additional DNA repair components that interact with Polo. In interphase, MRN recruits several effectors including MDC1 and C-terminal binding protein interacting protein (CtIP) to DSBs. Both MDC1 and CtIP are also found on mitotic DSBs (Giunta et al., 2010; Leimbacher et al., 2019; Wang et al., 2018). In addition, MDC1 interacts with TopBP1 on damaged chromosomes where they form filaments reminiscent of the Polo-coated tethers observed in *Drosophila* (Leimbacher et al., 2019; Royou et al., 2010). Importantly, systematic human interactome studies revealed an interaction between Plk1 and TopBP1 (Huttlin et al., 2015). Moreover, recent studies reported that the presence of DSBs in nocodazole-treated human cells triggers the Plk1-dependent phosphorylation of CtIP (Li et al., 2017). Therefore, it is possible that the MRN complex mediates the recruitment of Polo to DSBs indirectly by promoting the accumulation of one of its substrates such as TopBP1 or CtIP. The fact that Polo is maintained at DSBs until mid-anaphase or in prolonged prometaphase, at a time when MRN has already dissociated from DSBs, supports the notion that MRN is required for the initiation of Polo recruitment to mitotic DSBs but, unlike Cdk1, is dispensable for its maintenance.

Future studies will determine the molecular mechanisms by which MRN and Cdk1 control Polo association with mitotic DSBs and how Polo, in turn, facilitates the recruitment of BubR1/Bub3 to broken chromosomes. Current anti-cancer therapies rely heavily on the induction of extensive DNA damage, either by IR or genotoxic agents. Thus, deciphering the molecular pathways that process DNA damage in healthy mitotic cells will improve our understanding of tumor resistance to these therapies and may help identify novel targets that will enhance the efficacy of these therapies.

MATERIALS AND METHODS
Fly strains
Flies were grown on corn flour and yeast extract medium under standard conditions at 25°C. The h2az>H2A.Z::mRFP stock was obtained from the Bloomington *Drosophila* Stock Center (Indiana University, USA).

bub3>EGFP::Bub3 stock was provided by Christian Lehner (Institute of Molecular Sciences, University of Zurich, Switzerland). The bubR1>GFP::BubR1 stock was provided by R. Karess (Institute Jacques Monod, Paris, France). The polo>GFP::Polo stock was provided by Claudio Sunkel (Instituto de Biologia Molecular e Cellular, Porto, Portugal). The ubi>GFP::Fzy stock was provided by Jordan Raff (Sir William Dunn School of Pathology, University of Oxford, UK). The GFP::Jupiter is described by Karpova et al. (2006). The *bubR1[1]* (Basu et al., 1999), *polo[10]* (Donaldson et al., 2001) and *rad50[EP1]* (Ciapponi et al., 2004; Gorski et al., 2004) mutations were previously described. The transgenic stocks ubi>GFP::Mre11, ubi>GFP::LacI::Mre11, ubi>mRFP::Rad50, ubi>Okra::GFP and polo>mCherry::Polo were produced in our laboratory. The transgenic stock ubi>GFP::Mre11 and ubi>mRFP::Rad50 are described by Murcia et al. (2019).

Molecular cloning
All plasmids were verified by sequencing before being injected into fly embryos to generate transgenic stocks (Bestgene Inc.).

ubi>GFP::LacI::Mre11 cloning
The LacI sequence was amplified from the pGEX6p2 vector using primers that added the AttB1 and AttB2 Gateway sequences and the sequence of a GAGAGAGA flexible peptide linker to the N and C termini of LacI, respectively. The Mre11 coding sequence was amplified from pENTR-N-Mre11 vector with primers that added the GAGAGAGA linker and the AttB1 and AttB2 Gateway sequences on N and C termini of Mre11, respectively. The two PCR products were combined and amplified to get the final PCR product that was inserted into the entry Gateway vector. This product was recombined with a pUbi-GFP::GAT destination vector (a gift from Jordan Raff) to obtain the plasmid ubi>GFP::LacI::Mre11.

ubi>Okra::GFP cloning
The Okra coding sequence was amplified from the pOT2-Okr vector (DGRC, plasmid n°LD35220) using primers that added the AttB1 and AttB2 Gateway sequences on the N and C termini of Okra, respectively. The PCR product was inserted into the pDONR/Zeo vector (Life technologies). This resulting entry vector was recombined into the pUbi-GAT::GFP vector containing the ubiquitin promoter and a C-terminal GFP tag (a gift from Jordan Raff).

polo>mCherry::Polo cloning
The polo>mCherry::Polo construct was obtained by multistep cloning. First, a region of 881 nucleotides upstream of the Polo initiation codon was amplified from genomic DNA using primers introducing *Bam*HI and *Eco*RI restriction sites. mCherry was amplified with a forward primer introducing an *Eco*RI restriction site and a reverse primer introducing a *Not*I site plus a GAGAGAGA linker. The cDNA Polo sequence was amplified with forward and reverse primers introducing *Not*I and *Kpn*I sites, respectively. A region of 704 nucleotides after the STOP codon of PoloCDS was amplified from genomic DNA using forward and reverse primers introducing *Xho*I and *Kpn*I sites, respectively. Each PCR product was first inserted into a pGEM-T easy vector. After digestion, the products were ligated into a pAttB vector. Ligation of this product resulted in the final pAttB polo>mCherry::Polo vector.

Live analysis of larval neuroblasts
For live imaging of neuroblasts, late third-instar larvae were dissected in PBS (phosphate buffer saline, 1×) and their central nervous system transferred in a drop of PBS on a coverslip. The brain was gently compressed by capillary action and the coverslip sealed with Halocarbon oil 700 (Sigma). Each preparation was monitored for less than 1 h. For colchicine and BI2536 treatments, whole brains were incubated in PBS containing 10 μM colchicine (Sigma) and/or 1 μM BI2536 (Selleckchem) for 30 min before preparation for live imaging as described above. These conditions for colchicine and BI2536 treatment were optimal to produce >30 min delay in prometaphase. Live analysis was performed at room temperature with a 100× oil Plan-Apochromat objective lens (NA 1.4) and an Axio-Observed.Z1 microscope (Carl Zeiss) equipped with a spinning disk

confocal (Yokogawa), an EMCCD Evolve camera (Photometrics and Roper Scientific) and 491 nm (100 mW; Cobolt calypso) and 561 nm (100 mW; Cobolt Jive) lasers. Images were acquired with Metamorph software (Roper Scientific). Every 5 and/or 20 s, 12 Z-series of 0.5 μm steps were acquired. All images are maximum-intensity projections. A 355 nm microchip laser (Teem Photonics) (passively Q-switched SNV-20F-000) with a 21 kHz repetition rate, 0.8 μJ energy/pulse, 2 kW of peak power and 400 ps pulse width, powered with an iLas2 PULSE system (Roper Scientific) was used at 10, 15, 20 or 30% power with one pulse of a spot length of 100 points to induce surgical damage to one chromosome. For all experiments, 20% laser power was used unless specified otherwise.

Data analysis and quantification

ImageJ (Fiji, National Institutes of Health) was used for image analysis and fluorescence quantification. The level of our fluorescence-tagged proteins at DNA lesions was measured as follows: The average fluorescence intensity of a defined region of interest at the site of IR (ROI A) and the average fluorescence intensity of the cytoplasm near the site of IR (ROI B) were measured over time from maximum projection images (12z of 0.5 μm depth). The background of the camera was removed for each value. For each time point, the level of signal at the site of damage was equal to the difference between the average signal of ROIs A and B divided by the average signal in ROI B {[(ROI A-background)−(ROI B-background)]/(ROIB-background)}. The initiation of recruitment at DNA lesions corresponds to the time where the difference between ROI A and B signals is positive. To determine the half-time of recruitment ($t_{1/2}$) and maximum level parameters, each data set (from 0 min to the time of peak level) was fitted to the following sigmoid function: $Y=Max/\{1+10^{[((t1/2)-X)\times Hillslope]}\}$ using Prism (Graphpad), where Max is the maximum level. To estimate the half-time of dissociation, each data set was normalized to Max=1 and the data from $Y=1$ to the bottom plateau was fitted to the following sigmoid function: $Y=Bottom+(1-Bottom)/\{1+10^{[((t1/2)-X)\times Hillslope]}\}$. In Fig. 1H, Fig. 4B,C and Fig. 6G, the data were normalized to Max=1.

References
Ahmad, K. and Golic, K. G. (1998). The transmission of fragmented chromosomes in *Drosophila* melanogaster. *Genetics* **148**, 775-792.

Aleksandrov, R., Dotchev, A., Poser, I., Krastev, D., Georgiev, G., Panova, G., Babukov, Y., Danovski, G., Dyankova, T., Hubatsch, L. et al. (2018). Protein dynamics in complex DNA lesions. *Mol. Cell* **69**, 1046-1061.e1045. doi:10.1016/j.molcel.2018.02.016

Archambault, V., Lépine, G. and Kachaner, D. (2015). Understanding the Polo Kinase machine. *Oncogene* **34**, 4799-4807. doi:10.1038/onc.2014.451

Ayra-Plasencia, J. and Machín, F. (2019). Yeast cells can partially revert chromosome segregation to repair late DNA double-strand breaks through homologous recombination. *Mol. Cell Oncol.* **6**, e1648027. doi:10.1080/23723556.2019.1648027

Basu, J., Logarinho, E., Herrmann, S., Bousbaa, H., Li, Z. X., Chan, G. K. T., Yen, T. J., Sunkel, C. E. and Goldberg, M. L. (1998). Localization of the *Drosophila* checkpoint control protein Bub3 to the kinetochore requires Bub1 but not Zw10 or Rod. *Chromosoma* **107**, 376-385. doi:10.1007/s004120050321

Basu, J., Bousbaa, H., Logarinho, E., Li, Z. X., Williams, B. C., Lopes, C., Sunkel, C. E. and Goldberg, M. L. (1999). Mutations in the essential spindle checkpoint gene bub1 cause chromosome missegregation and fail to block apoptosis in *Drosophila*. *J. Cell Biol.* **146**, 13-28. doi:10.1083/jcb.146.1.13

Belmont, A. S. and Straight, A. F. (1998). In vivo visualization of chromosomes using lac operator-repressor binding. *Trends Cell Biol.* **8**, 121-124. doi:10.1016/S0962-8924(97)01211-7

Benada, J., Burdová, K., Lidak, T., von Morgen, P. and Macurek, L. (2015). Polo-like kinase 1 inhibits DNA damage response during mitosis. *Cell Cycle* **14**, 219-231. doi:10.4161/15384101.2014.977067

Bhandari, J., Karg, T. and Golic, K. G. (2019). Homolog-dependent repair following dicentric chromosome breakage in *Drosophila* melanogaster. *Genetics* **212**, 615-630. doi:10.1534/genetics.119.302247

Blackford, A. N. and Stucki, M. (2020). How cells respond to DNA breaks in mitosis. *Trends Biochem. Sci.* **45**, 321-331. doi:10.1016/j.tibs.2019.12.010

Blower, M. D. and Karpen, G. H. (2001). The role of *Drosophila* CID in kinetochore formation, cell-cycle progression and heterochromatin interactions. *Nat. Cell Biol.* **3**, 730-739. doi:10.1038/35087045

Bonilla, C. Y., Melo, J. A. and Toczyski, D. P. (2008). Colocalization of sensors is sufficient to activate the DNA damage checkpoint in the absence of damage. *Mol. Cell* **30**, 267-276. doi:10.1016/j.molcel.2008.03.023

Cannan, W. J. and Pederson, D. S. (2016). Mechanisms and consequences of double-strand DNA break formation in chromatin. *J. Cell. Physiol.* **231**, 3-14. doi:10.1002/jcp.25048

Ceccaldi, R., Rondinelli, B. and D'Andrea, A. D. (2016). Repair pathway choices and consequences at the double-strand break. *Trends Cell Biol.* **26**, 52-64. doi:10.1016/j.tcb.2015.07.009

Ciapponi, L., Cenci, G., Ducau, J., Flores, C., Johnson-Schlitz, D., Gorski, M. M., Engels, W. R. and Gatti, M. (2004). The *Drosophila* Mre11/Rad50 complex is required to prevent both telomeric fusion and chromosome breakage. *Curr. Biol.* **14**, 1360-1366. doi:10.1016/j.cub.2004.07.019

Ciapponi, L., Cenci, G. and Gatti, M. (2006). The *Drosophila* Nbs protein functions in multiple pathways for the maintenance of genome stability. *Genetics* **173**, 1447-1454. doi:10.1534/genetics.106.058081

Conde, C., Osswald, M., Barbosa, J., Moutinho-Santos, T., Pinheiro, D., Guimarães, S., Matos, I., Maiato, H. and Sunkel, C. E. (2013). *Drosophila* Polo regulates the spindle assembly checkpoint through Mps1-dependent BubR1 phosphorylation. *EMBO J.* **32**, 1761-1777. doi:10.1038/emboj.2013.109

Derive, N., Landmann, C., Montembault, E., Claverie, M.-C., Pierre-Elies, P., Goutte-Gattat, D., Founounou, N., McCusker, D. and Royou, A. (2015). Bub3-BubR1-dependent sequestration of Cdc20Fizzy at DNA breaks facilitates the correct segregation of broken chromosomes. *J. Cell Biol.* **211**, 517-532. doi:10.1083/jcb.201504059

Donaldson, M. M., Tavares, A. M., Ohkura, H., Deak, P. and Glover, D. M. (2001). Metaphase arrest with centromere separation in polo mutants of *Drosophila*. *J. Cell Biol.* **153**, 663-676. doi:10.1083/jcb.153.4.663

Dronamraju, R. and Mason, J. M. (2009). Recognition of double strand breaks by a mutator protein (MU2) in *Drosophila* melanogaster. *PLoS Genet.* **5**, e1000473. doi:10.1371/journal.pgen.1000473

Elia, A. E. H., Cantley, L. C. and Yaffe, M. B. (2003a). Proteomic screen finds pSer/pThr-binding domain localizing Plk1 to mitotic substrates. *Science* **299**, 1228-1231. doi:10.1126/science.1079079

Elia, A. E. H., Rellos, P., Haire, L. F., Chao, J. W., Ivins, F. J., Hoepker, K., Mohammad, D., Cantley, L. C., Smerdon, S. J. and Yaffe, M. B. (2003b). The molecular basis for phosphodependent substrate targeting and regulation of Plks by the Polo-box domain. *Cell* **115**, 83-95. doi:10.1016/S0092-8674(03)00725-6

Espert, A., Uluocak, P., Bastos, R. N., Mangat, D., Graab, P. and Gruneberg, U. (2014). PP2A-B56 opposes Mps1 phosphorylation of Knl1 and thereby promotes spindle assembly checkpoint silencing. *J. Cell Biol.* **206**, 833-842. doi:10.1083/jcb.201406109

Espeut, J., Lara-Gonzalez, P., Sassine, M., Shiau, A. K., Desai, A. and Abrieu, A. (2015). Natural loss of Mps1 kinase in nematodes uncovers a role for polo-like kinase 1 in spindle checkpoint initiation. *Cell Rep.* **12**, 58-65. doi:10.1016/j.celrep.2015.05.039

Falck, J., Coates, J. and Jackson, S. P. (2005). Conserved modes of recruitment of ATM, ATR and DNA-PKcs to sites of DNA damage. *Nature* **434**, 605-611. doi:10.1038/nature03442

Giunta, S., Belotserkovskaya, R. and Jackson, S. P. (2010). DNA damage signaling in response to double-strand breaks during mitosis. *J. Cell Biol.* **190**, 197-207. doi:10.1083/jcb.200911156

Gomez-Godinez, V., Wu, T., Sherman, A. J., Lee, C. S., Liaw, L.-H., Zhongsheng, Y., Yokomori, K. and Berns, M. W. (2010). Analysis of DNA double-strand break response and chromatin structure in mitosis using laser microirradiation. *Nucleic Acids Res.* **38**, e202. doi:10.1093/nar/gkq836

Gorski, M. M., Romeijn, R. J., Eeken, J. C. J., de Jong, A. W. M., van Veen, B. L., Szuhai, K., Mullenders, L. H., Ferro, W. and Pastink, A. (2004). Disruption of Drosophila Rad50 causes pupal lethality, the accumulation of DNA double-strand breaks and the induction of apoptosis in third instar larvae. DNA Repair 3, 603-615. doi:10.1016/j.dnarep.2004.02.001

Haber, J. E. and Thorburn, P. C. (1984). Healing of broken linear dicentric chromosomes in yeast. Genetics 106, 207-226.

Hartlerode, A. J. and Scully, R. (2009). Mechanisms of double-strand break repair in somatic mammalian cells. Biochem. J. 423, 157-168. doi:10.1042/BJ20090942

Huttlin, E. L., Ting, L., Bruckner, R. J., Gebreab, F., Gygi, M. P., Szpyt, J., Tam, S., Zarraga, G., Colby, G., Baltier, K. et al. (2015). The BioPlex network: a systematic exploration of the human interactome. Cell 162, 425-440. doi:10.1016/j.cell.2015.06.043

Jackson, S. P. and Bartek, J. (2009). The DNA-damage response in human biology and disease. Nature 461, 1071-1078. doi:10.1038/nature08467

Kang, Y. H., Park, J.-E., Yu, L.-R., Soung, N.-K., Yun, S.-M., Bang, J. K., Seong, Y.-S., Yu, H., Garfield, S., Veenstra, T. D. et al. (2006). Self-regulated Plk1 recruitment to kinetochores by the Plk1-PBIP1 interaction is critical for proper chromosome segregation. Mol. Cell 24, 409-422. doi:10.1016/j.molcel.2006.10.016

Karess, R. E., Wassmann, K. and Rahmani, Z. (2013). New insights into the role of BubR1 in mitosis and beyond. Int. Rev. Cell Mol. Biol. 306, 223-273. doi:10.1016/B978-0-12-407694-5.00006-7

Karpova, N., Bobinnec, Y., Fouix, S., Huitorel, P. and Debec, A. (2006). Jupiter, a new Drosophila protein associated with microtubules. Cell Motil. Cytoskeleton 63, 301-312. doi:10.1002/cm.20124

Kooistra, R., Pastink, A., Zonneveld, J. B. M., Lohman, P. H. M. and Eeken, J. C. J. (1999). The Drosophila melanogaster DmRAD54 gene plays a crucial role in double-strand break repair after P-element excision and acts synergistically with Ku70 in the repair of X-ray damage. Mol. Cell. Biol. 19, 6269-6275. doi:10.1128/MCB.19.9.6269

Kruse, T., Zhang, G., Larsen, M. S. Y., Lischetti, T., Streicher, W., Kragh Nielsen, T., Bjorn, S. P. and Nilsson, J. (2013). Direct binding between BubR1 and B56-PP2A phosphatase complexes regulate mitotic progression. J. Cell Sci. 126, 1086-1092. doi:10.1242/jcs.122481

Leimbacher, P.-A., Jones, S. E., Shorrocks, A.-M. K., de Marco Zompit, M., Day, M., Blaauwendraad, J., Bundschuh, D., Bonham, S., Fischer, R., Fink, D. et al. (2019). MDC1 interacts with TOPBP1 to maintain chromosomal stability during mitosis. Mol. Cell 74, 571-583.e578. doi:10.1016/j.molcel.2019.02.014

Lénárt, P., Petronczki, M., Steegmaier, M., Di Fiore, B., Lipp, J. J., Hoffmann, M., Rettig, W. J., Kraut, N. and Peters, J.-M. (2007). The small-molecule inhibitor BI 2536 reveals novel insights into mitotic roles of polo-like kinase 1. Curr. Biol. 17, 304-315. doi:10.1016/j.cub.2006.12.046

Li, Z., Li, J., Kong, Y., Yan, S., Ahmad, N. and Liu, X. (2017). Plk1 phosphorylation of Mre11 antagonizes the DNA damage response. Cancer Res. 77, 3169-3180. doi:10.1158/0008-5472.CAN-16-2787

Lisby, M., Barlow, J. H., Burgess, R. C. and Rothstein, R. (2004). Choreography of the DNA damage response: spatiotemporal relationships among checkpoint and repair proteins. Cell 118, 699-713. doi:10.1016/j.cell.2004.08.015

Llamazares, S., Moreira, A., Tavares, A., Girdham, C., Spruce, B. A., Gonzalez, C., Karess, R. E., Glover, D. M. and Sunkel, C. E. (1991). polo encodes a protein kinase homolog required for mitosis in Drosophila. Genes Dev. 5, 2153-2165. doi:10.1101/gad.5.12a.2153

Lopes, C. S., Sampaio, P., Williams, B., Goldberg, M. and Sunkel, C. E. (2005). The Drosophila Bub3 protein is required for the mitotic checkpoint and for normal accumulation of cyclins during G2 and early stages of mitosis. J. Cell Sci. 118, 187-198. doi:10.1242/jcs.01602

Lowery, D. M., Lim, D. and Yaffe, M. B. (2005). Structure and function of Polo-like kinases. Oncogene 24, 248-259. doi:10.1038/sj.onc.1208280

Lukas, C., Falck, J., Bartkova, J., Bartek, J. and Lukas, J. (2003). Distinct spatiotemporal dynamics of mammalian checkpoint regulators induced by DNA damage. Nat. Cell Biol. 5, 255-260. doi:10.1038/ncb945

Lukas, C., Melander, F., Stucki, M., Falck, J., Bekker-Jensen, S., Goldberg, M., Lerenthal, Y., Jackson, S. P., Bartek, J. and Lukas, J. (2004). Mdc1 couples DNA double-strand break recognition by Nbs1 with its H2AX-dependent chromatin retention. EMBO J. 23, 2674-2683. doi:10.1038/sj.emboj.7600269

McClintock, B. (1938). The fusion of broken ends of sister half-chromatids following breakage at meiotic anaphase. Missouri Agric. Exp. Station Res. Bull. 290, 1-48.

McClintock, B. (1939). The behavior in successive nuclear divisions of a chromosome broken at meiosis. Proc. Natl. Acad. Sci. USA 25, 405-416. doi:10.1073/pnas.25.8.405

McClintock, B. (1941). The stability of broken ends of chromosomes in Zea Mays. Genetics 26, 234-282.

Melo, J. and Toczyski, D. (2002). A unified view of the DNA-damage checkpoint. Curr. Opin. Cell Biol. 14, 237-245. doi:10.1016/S0955-0674(02)00312-5

Montembault, E., Claverie, M.-C., Bouit, L., Landmann, C., Jenkins, J., Tsankova, A., Cabernard, C. and Royou, A. (2017). Myosin efflux promotes cell elongation to coordinate chromosome segregation with cell cleavage. Nat. Commun. 8, 326. doi:10.1038/s41467-017-00337-6

Mortensen, E. M., Haas, W., Gygi, M., Gygi, S. P. and Kellogg, D. R. (2005). Cdc28-dependent regulation of the Cdc5/Polo kinase. Curr. Biol. 15, 2033-2037. doi:10.1016/j.cub.2005.10.046

Murcia, L., Clemente-Ruiz, M., Pierre-Elies, P., Royou, A. and Milán, M. (2019). Selective killing of RAS-malignant tissues by exploiting oncogene-induced DNA damage. Cell Rep. 28, 119-131.e114. doi:10.1016/j.celrep.2019.06.004

Myler, L. R., Gallardo, I. F., Soniat, M. M., Deshpande, R. A., Gonzalez, X. B., Kim, Y., Paull, T. T. and Finkelstein, I. J. (2017). Single-molecule imaging reveals how Mre11-Rad50-Nbs1 initiates DNA break repair. Mol. Cell 67, 891-898.e894. doi:10.1016/j.molcel.2017.08.002

Orthwein, A., Fradet-Turcotte, A., Noordermeer, S. M., Canny, M. D., Brun, C. M., Strecker, J., Escribano-Diaz, C. and Durocher, D. (2014). Mitosis inhibits DNA double-strand break repair to guard against telomere fusions. Science 344, 189-193. doi:10.1126/science.1248024

Peterson, S. E., Li, Y., Chait, B. T., Gottesman, M. E., Baer, R. and Gautier, J. (2011). Cdk1 uncouples CtIP-dependent resection and Rad51 filament formation during M-phase double-strand break repair. J. Cell Biol. 194, 705-720. doi:10.1083/jcb.201103103

Polo, S. E. and Jackson, S. P. (2011). Dynamics of DNA damage response proteins at DNA breaks: a focus on protein modifications. Genes Dev. 25, 409-433. doi:10.1101/gad.2021311

Primorac, I., Weir, J. R., Chiroli, E., Gross, F., Hoffmann, I., van Gerwen, S., Ciliberto, A. and Musacchio, A. (2013). Bub3 reads phosphorylated MELT repeats to promote spindle assembly checkpoint signaling. eLife 2, e01030. doi:10.7554/eLife.01030

Riparbelli, M. G., Gottardo, M., Glover, D. M. and Callaini, G. (2014). Inhibition of Polo kinase by BI2536 affects centriole separation during Drosophila male meiosis. Cell Cycle 13, 2064-22632. doi:10.4161/cc.29083

Rogakou, E. P., Pilch, D. R., Orr, A. H., Ivanova, V. S. and Bonner, W. M. (1998). DNA double-stranded breaks induce histone H2AX phosphorylation on serine 139. J. Biol. Chem. 273, 5858-5868. doi:10.1074/jbc.273.10.5858

Royou, A., Gagou, M. E., Karess, R. and Sullivan, W. (2010). BubR1- and polo-coated DNA tethers facilitate poleward segregation of acentric chromatids. Cell 140, 235-245. doi:10.1016/j.cell.2009.12.043

Schmucker, S. and Sumara, I. (2014). Molecular dynamics of PLK1 during mitosis. Mol. Cell Oncol. 1, e954507. doi:10.1080/23723548.2014.954507

Schupbach, T. and Wieschaus, E. (1991). Female sterile mutations on the second chromosome of Drosophila melanogaster. II. Mutations blocking oogenesis or altering egg morphology. Genetics 129, 1119-1136.

Sekelsky, J. (2017). DNA repair in Drosophila: mutagens, models, and missing genes. Genetics 205, 471-490. doi:10.1534/genetics.116.186759

Silva, B. A., Stambaugh, J. R., Yokomori, K., Shah, J. V. and Berns, M. W. (2014). DNA damage to a single chromosome end delays anaphase onset. J. Biol. Chem. 289, 22771-22784. doi:10.1074/jbc.M113.535955

Soutoglou, E. and Misteli, T. (2008). Activation of the cellular DNA damage response in the absence of DNA lesions. Science 320, 1507-1510. doi:10.1126/science.1159051

Steegmaier, M., Hoffmann, M., Baum, A., Lénárt, P., Petronczki, M., Kršššák, M., Gürtler, U., Garin-Chesa, P., Lieb, S., Quant, J. et al. (2007). BI 2536, a potent and selective inhibitor of polo-like kinase 1, inhibits tumor growth in vivo. Curr. Biol. 17, 316-322. doi:10.1016/j.cub.2006.12.037

Stewart, G. S., Wang, B., Bignell, C. R., Taylor, A. M. R. and Elledge, S. J. (2003). MDC1 is a mediator of the mammalian DNA damage checkpoint. Nature 421, 961-966. doi:10.1038/nature01446

Stucki, M., Clapperton, J. A., Mohammad, D., Yaffe, M. B., Smerdon, S. J. and Jackson, S. P. (2005). MDC1 directly binds phosphorylated histone H2AX to regulate cellular responses to DNA double-strand breaks. Cell 123, 1213-1226. doi:10.1016/j.cell.2005.09.038

Suijkerbuijk, S. J. E., Vleugel, M., Teixeira, A. and Kops, G. J. P. L. (2012). Integration of kinase and phosphatase activities by BUBR1 ensures formation of stable kinetochore-microtubule attachments. Dev. Cell 23, 745-755. doi:10.1016/j.devcel.2012.09.005

Sumara, I., Giménez-Abián, J. F., Gerlich, D., Hirota, T., Kraft, C., de la Torre, C., Ellenberg, J. and Peters, J.-M. (2004). Roles of polo-like kinase 1 in the assembly of functional mitotic spindles. Curr. Biol. 14, 1712-1722. doi:10.1016/j.cub.2004.09.049

Sunkel, C. E. and Glover, D. M. (1988). polo, a mitotic mutant of Drosophila displaying abnormal spindle poles. J. Cell Sci. 89, 25-38.

Syed, A. and Tainer, J. A. (2018). The MRE11-RAD50-NBS1 complex conducts the orchestration of damage signaling and outcomes to stress in DNA replication and repair. Annu. Rev. Biochem. 87, 263-294. doi:10.1146/annurev-biochem-062917-012415

Terasawa, M., Shinohara, A. and Shinohara, M. (2014). Canonical non-homologous end joining in mitosis induces genome instability and is suppressed by M-phase-specific phosphorylation of XRCC4. PLoS Genet. 10, e1004563. doi:10.1371/journal.pgen.1004563

Thompson, R., Gatenby, R. and Sidi, S. (2019). How cells handle DNA breaks during mitosis: detection, signaling, repair, and fate choice. Cells 8, 1049. doi:10.3390/cells8091049

van Vugt, M. A. T. M., Gardino, A. K., Linding, R., Ostheimer, G. J., Reinhardt, H. C., Ong, S.-E., Tan, C. S., Miao, H., Keezer, S. M., Li, J. et al. (2010). A mitotic phosphorylation feedback network connects Cdk1, Plk1, 53BP1, and Chk2 to inactivate the G(2)/M DNA damage checkpoint. *PLoS Biol.* **8**, e1000287. doi:10. 1371/journal.pbio.1000287

Wang, H., Qiu, Z., Liu, B., Wu, Y., Ren, J., Liu, Y., Zhao, Y., Wang, Y., Hao, S., Li, Z. et al. (2018). PLK1 targets CtIP to promote microhomology-mediated end joining. *Nucleic Acids Res.* **46**, 10724-10739. doi:10.1093/nar/gky810

Williams, G. J., Lees-Miller, S. P. and Tainer, J. A. (2010). Mre11-Rad50-Nbs1 conformations and the control of sensing, signaling, and effector responses at DNA double-strand breaks. *DNA Repair* **9**, 1299-1306. doi:10.1016/j.dnarep. 2010.10.001

Wu, L., Luo, K., Lou, Z. and Chen, J. (2008). MDC1 regulates intra-S-phase checkpoint by targeting NBS1 to DNA double-strand breaks. *Proc. Natl. Acad. Sci. USA.* **105**, 11200-11205. doi:10.1073/pnas.0802885105

Xu, R., Xu, Y., Huo, W., Lv, Z., Yuan, J., Ning, S., Wang, Q., Hou, M., Gao, G., Ji, J. et al. (2018). Mitosis-specific MRN complex promotes a mitotic signaling cascade to regulate spindle dynamics and chromosome segregation. *Proc. Natl. Acad. Sci. USA* **115**, E10079-E10088. doi:10.1073/pnas.1806665115

Yu, B., Dalton, W. B. and Yang, V. W. (2012). CDK1 regulates mediator of DNA damage checkpoint 1 during mitotic DNA damage. *Cancer Res.* **72**, 5448-5453. doi:10.1158/0008-5472.CAN-12-2354

Zhai, B., Villén, J., Beausoleil, S. A., Mintseris, J. and Gygi, S. P. (2008). Phosphoproteome analysis of *Drosophila* melanogaster embryos. *J. Proteome Res.* **7**, 1675-1682. doi:10.1021/pr700696a

Supplementary figure 1

A

B

C

D

E
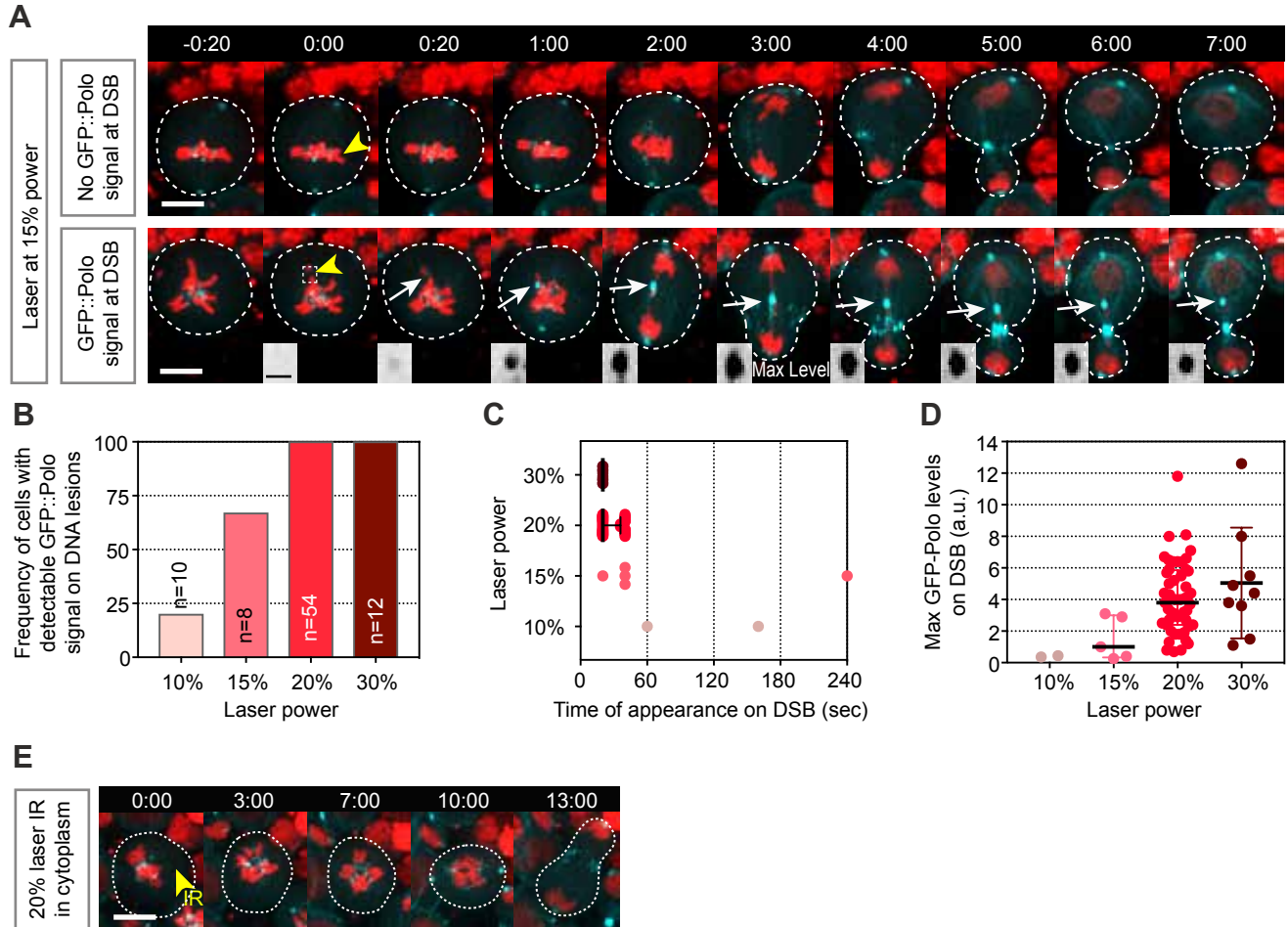
Figure S1. GFP::Polo kinetics at DSB induced by a pulsed UV laser used at different power percentages during mitosis. (**A**) Time-lapse images of neuroblasts expressing H2Az::mRFP (red) and GFP::Polo (cyan) before and after micro-irradiation (IR) of one chromosome with a 355 nm pulsed laser at 15% power. Yellow arrowheads indicate the site of IR. Time=min:sec. Time=0:00 corresponds to the time of IR. The top panels show a cell with no detectable GFP::Polo signal at the site of damage. The bottom panels show a cell where GFP::Polo signal is detected at the IR-induced DNA lesions (the white arrows and insets). The white dashed square represents the inset region. The insets show GFP::Polo inverted signal at the site of damage. Scale Bar=5 µm and 1 µm for panels and insets, respectively. (**B**) Graph showing the frequency of cells with a detectable GFP::Polo signal at the site of IR for the indicated conditions. (**C, D**) Scatter dot plots showing the time of appearance (**C**) and the maximum levels (**D**) of GFP::Polo for the indicated conditions. Lines represent median ± interquartile.

(**E**) Time-lapse images of a neuroblast expressing H2Az::mRFP (red) and GFP::Polo (cyan) after micro-irradiation (IR, yellow arrowheads) of defined zone in the cytoplasm. Time=min:sec. Time=0:00 corresponds to the time of IR. Scale Bar=5µm.

Supplementary figure 2
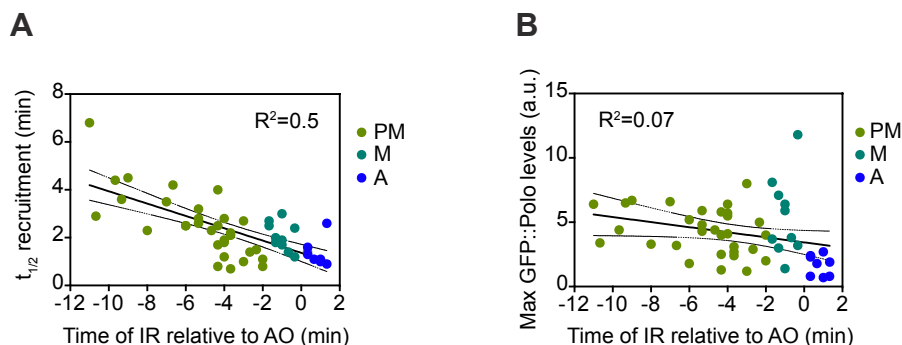
Figure S2. GFP::Polo kinetics at DSB induced at different stages of mitosis. (**A**) Graph showing the distribution of the $t_{1/2}$ of GFP::Polo recruitment to DSBs with the time of IR relative to anaphase onset (AO). PM, M and A correspond to cells where IR was applied in prometaphase, metaphase or anaphase respectively. A linear regression shows a correlation between the $t_{1/2}$ and the time of IR relative to AO. (**B**) Graph showing the distribution of GFP::Polo maximum levels at DSBs with the time of IR relative to anaphase onset (AO). PM, M and A correspond to cells where IR was applied in prometaphase, metaphase or anaphase respectively. A linear regression shows no correlation between maximum levels and the time elapsed between IR and AO. Lines correspond to mean±SD.

Supplementary figure 3
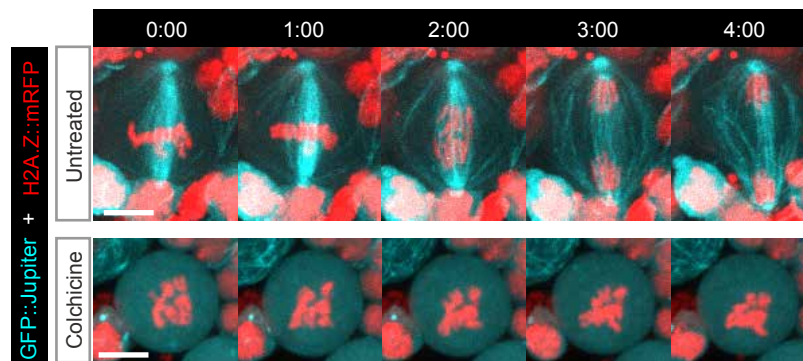
Figure S3. Complete depolymerisation of microtubules in mitotic neuroblasts upon colchicine treatment. Time-lapse images of neuroblasts expressing H2Az::mRFP (red) and the microtubule-binding protein GFP::Jupiter (cyan) after 30min incubation with PBS alone (untreated, top panels) or PBS plus 10µm colchicine (colchicine, bottom panels). Note the disappearance of the bipolar spindle after treatment with colchicine. Time: min:sec. Scale Bar=5 µm

Supplementary figure 4

A
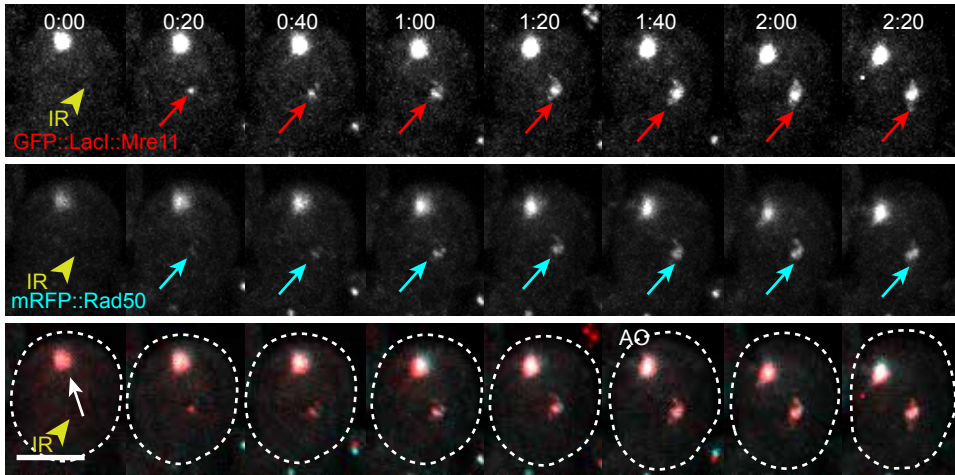
B
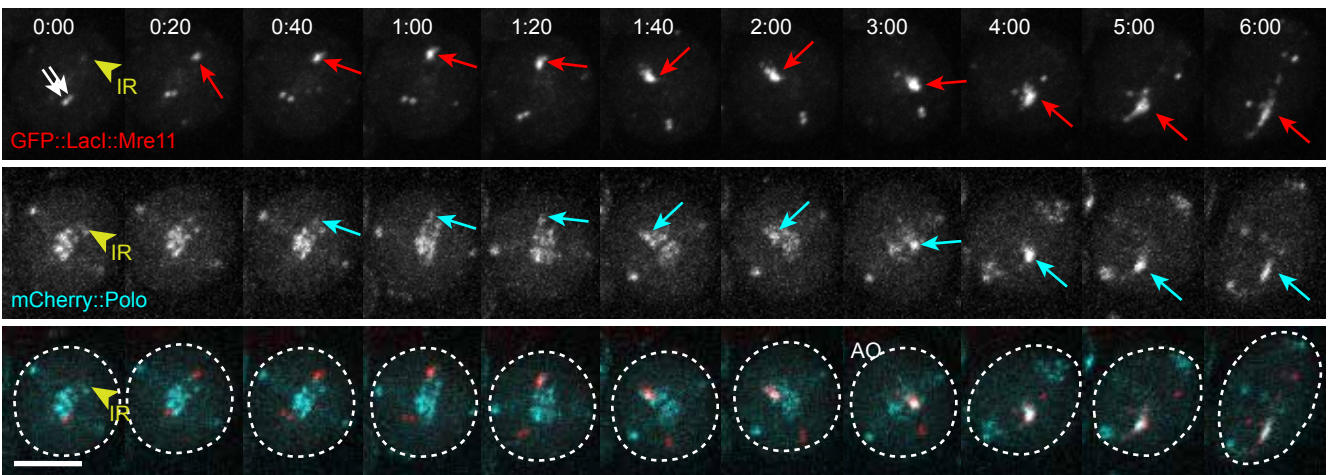
Figure S4. GFP::LacI::Mre11 co-localizes with mRFP::Rad50 on laser-induced DSBs during mitosis. (A) Time-lapse images of neuroblasts expressing GFP::LacI::Mre11 (top row, red in merge) and mRFP::Rad50 (middle row, cyan in merge) after microirradiation (IR). The yellow arrowheads indicate the site of IR. The red arrows point to the GFP::LacI::Mre11 signal on DSB and the cyan arrows indicate mRFP::Rad50 signal at DSBs. Note that GFP::LacI::Mre11 and mRFP::Rad50 signals were both detected on DSBs within 20 seconds following laser ablation. AO: anaphase onset. Time: min:sec. Scale Bar=5 µm. In neuroblasts expressing GFP::LacI::Mre11 and mRFP::Rad50, both proteins co-localize in a large cytoplasmic aggregate present in all cells (white arrow in merge). **(B)** Time-lapse images of neuroblasts expressing GFP::LacI::Mre11 (top row, red in merge) and mCherry::Polo (middle row, cyan in merge) and carrying LacO arrays on the X chromosome after IR. The yellow arrowheads indicate the site of IR. The red and white arrows indicate the GFP::LacI::Mre11 signal on the DNA lesions and LacO arrays respectively. The cyan arrows indicate mCherry::Polo signal at site of IR. Note that GFP::LacI::Mre11 is detected at the site of IR prior to mCherry::Polo (20 and 40sec respectively). AO: anaphase onset. Time=min:sec. Scale Bar=5 µm.

Supplementary figure 5
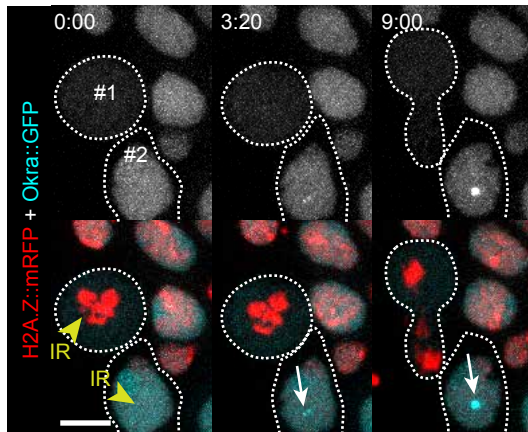
Figure S5. Okra does not localize on laser-induced DSBs during mitosis. Time lapse images of neuroblasts expressing H2A.Z::mRFP (red in merge) and Okra::GFP (gray in top row and cyan in merge) after microirradiation (IR). The yellow arrowheads indicate the site of IR. Cell #1 is in mitosis and cell #2 is in interphase. Cells are monitored within a few seconds after laser ablation (time 0:00). Okra::GFP signal appears after 3 minutes following IR in the interphase nucleus (white arrow). In contrast, no Okra::GFP signal is detected at the site of IR in mitotic cells. The white dashed lines highlight the contour of the cells. Time: min:sec. Scale Bar=5μm.
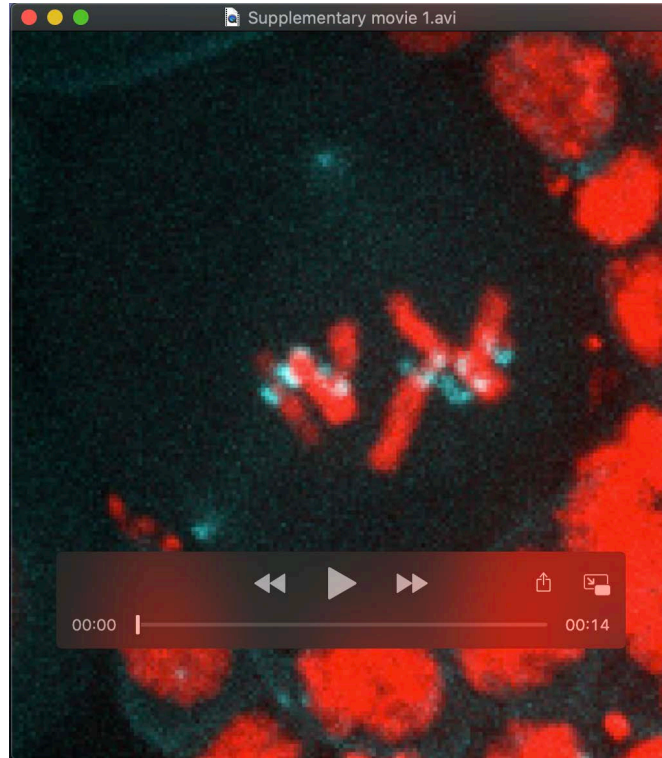
Movie 1. GFP::Polo kinetics at laser-induced DSBs created during prometaphase. Time-lapse video of wild type third instar larvae neuroblast expressing H2A.Z::mRFP (red) and GFP::Polo (Cyan). The first image represents the cell before microirradiation. The yellow arrow points to the site of microirradiation (IR). The white arrow indicates the appearance of GFP::Polo at the site of damage. Time 0:00 corresponds to the time of recording few seconds after microirradiation. Time=min:sec. Images are maximum projections. The movie corresponds to Fig. 1A (top panels).
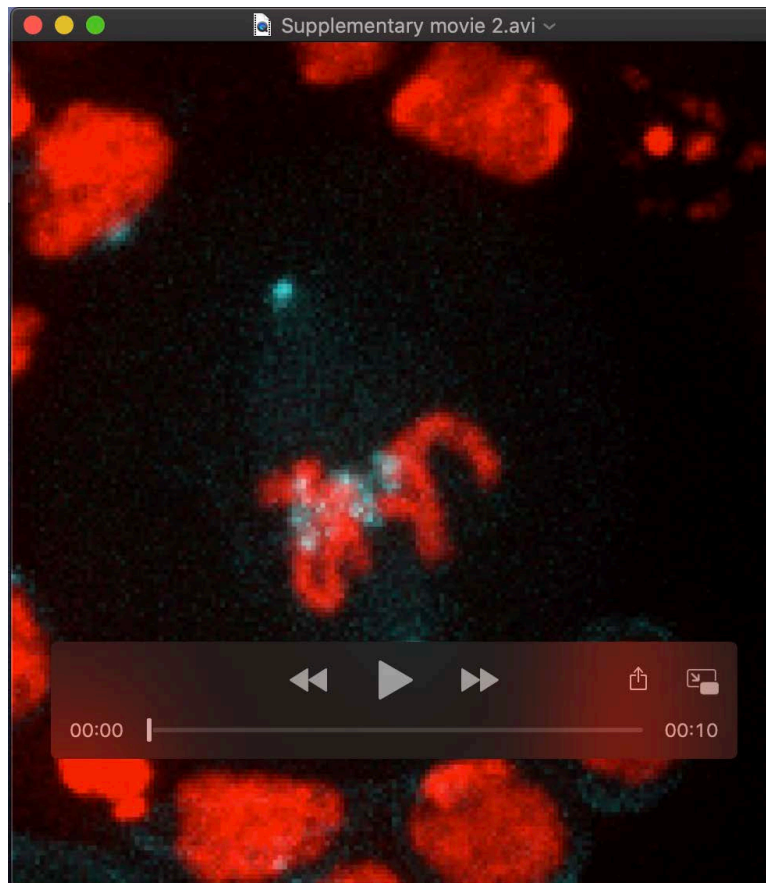
Movie 2: GFP::Polo kinetics at laser-induced DSBs created during metaphase. Time-lapse video of wild type neuroblast expressing H2A.Z::mRFP (red) and GFP::Polo (Cyan). The first image represents the cell before microirradiation (IR). The yellow arrow points to the site of microirradiation (IR). The white arrow indicates the appearance of GFP::Polo at the site of damage. Time 0:00 corresponds to the time of recording few seconds after IR. Time=min:sec. Images are maximum projections. The movie corresponds to Fig. 1A (middle panels).
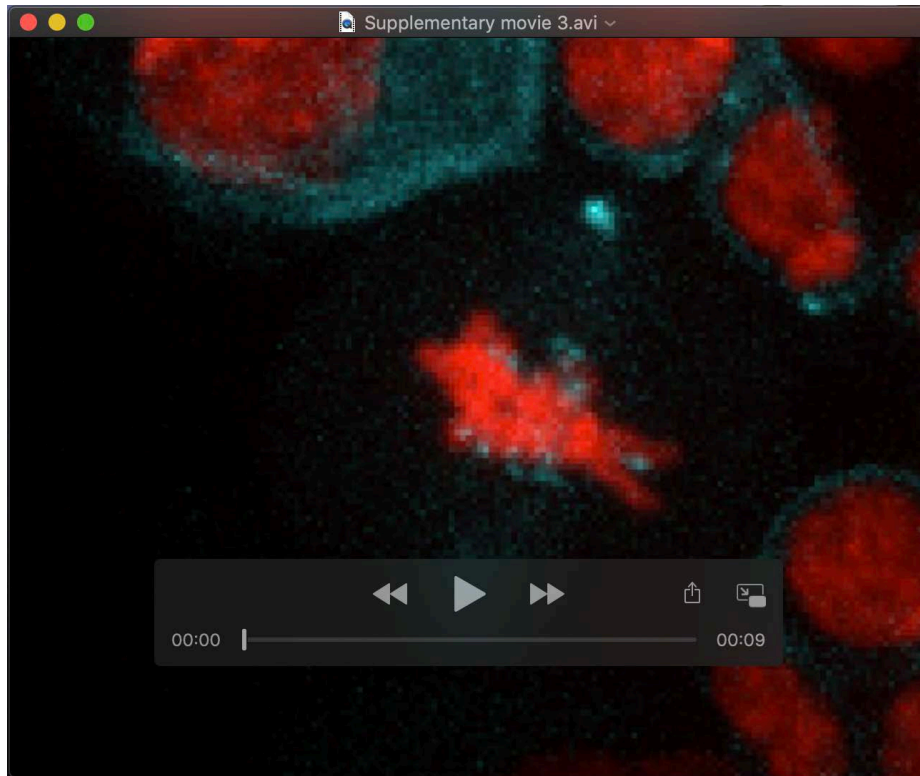
Movie 3: GFP::Polo kinetics at laser-induced DSBs created during anaphase. Time-lapse video of wild type neuroblast expressing H2A.Z::mRFP (red) and GFP::Polo (Cyan). The first image represents the cell before microirradiation (IR). The yellow arrow points to the site of irradiation (IR). The white arrow indicates the appearance of GFP::Polo at the site of damage. Time 0:00 corresponds to the time of recording few seconds after irradiation. Time=min:sec. Images are maximum projections. The movie corresponds to Fig. 1A (bottom panels).
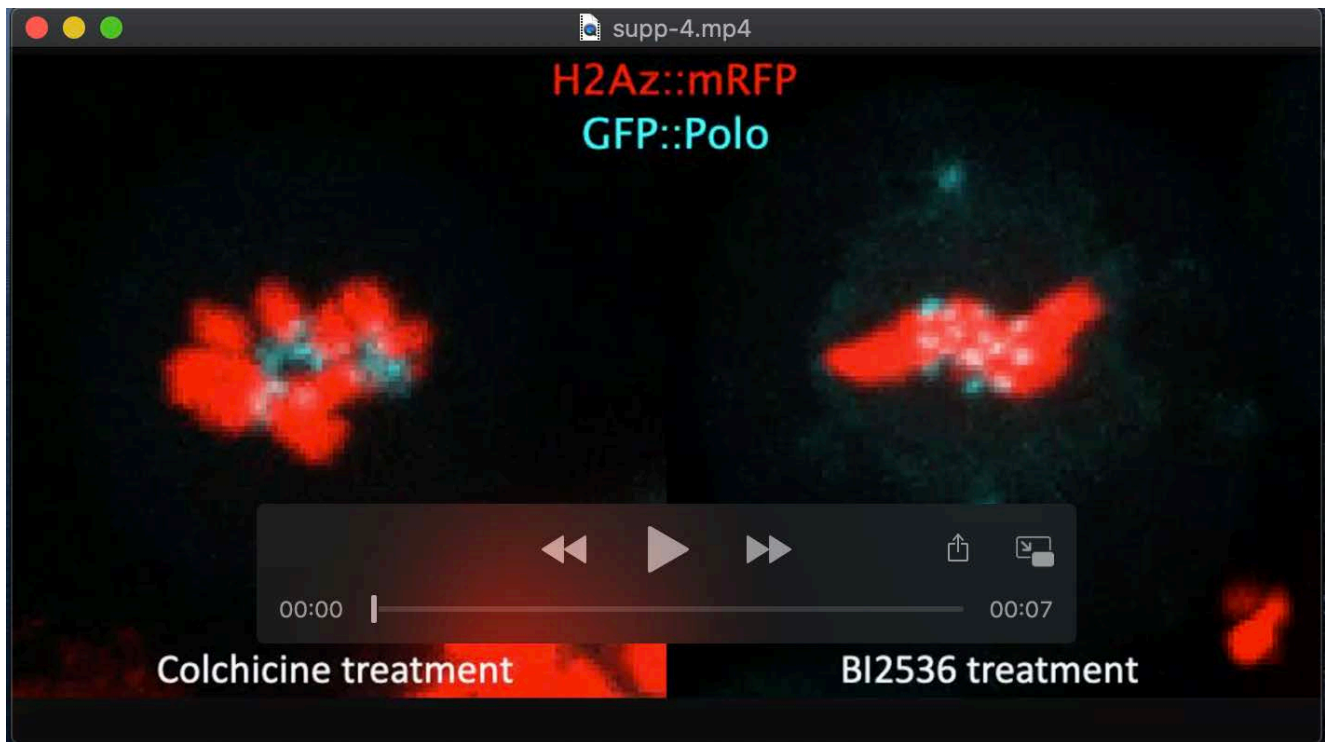
Movie 4: Polo kinase activity is required for its robust recruitment to mitotic DSBs. Time-lapse video of wild type neuroblast expressing H2A.Z::mRFP (red) and GFP::Polo (Cyan) previously treated with Colchicine (left panel) or BI2536 (right panel) for 30 minutes. The first image represents the cells before microirradiation (IR). The yellow arrows point to the site of irradiation (IR). The white arrows indicate the appearance of GFP::Polo at the site of damage for the indicated treatment. Time 0:00 corresponds to the time of recording few seconds after irradiation. Time=min:sec. Images are maximum projections. The movie corresponds to Fig. 2A.
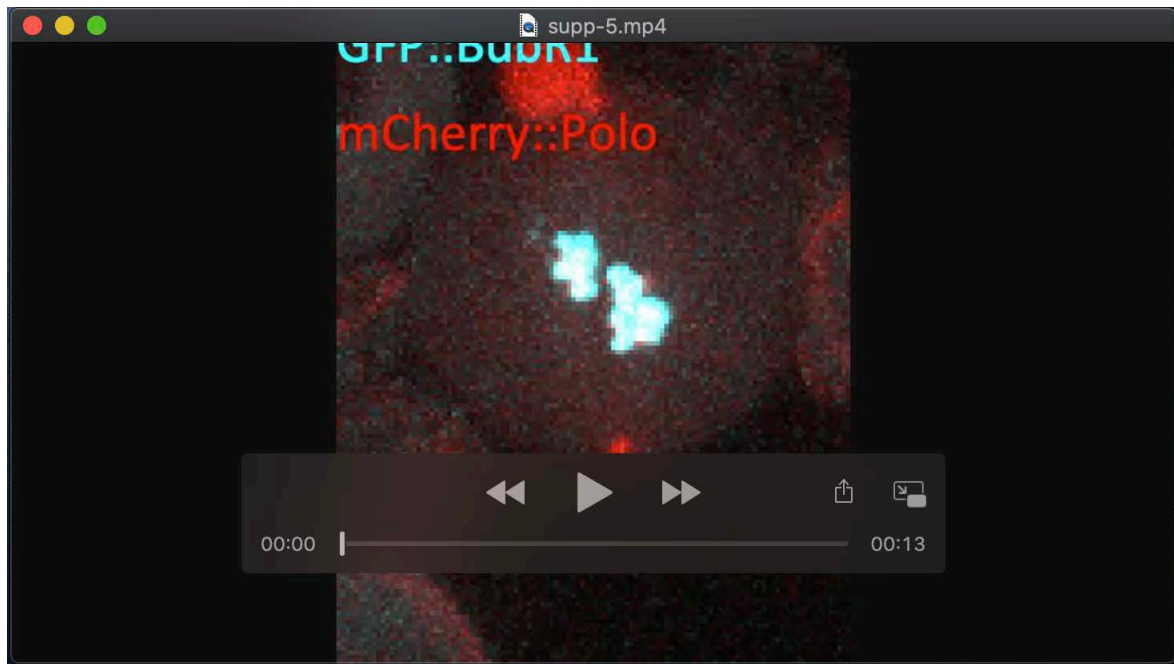
Movie 5: Kinetics of GFP::BubR1 and mCherry::Polo to DSBs during mitosis.

Time-lapse video of wild type neuroblast expressing GFP::BubR1 (Cyan) and mCherry::Polo The first image represents the cell before microirradiation (IR). The yellow arrows point to the site of IR. The red and cyan arrows indicate the appearance of mCherry::Polo and GFP::BubR1 respectively at the site of damage. Time 0:00 corresponds to the time of recording few seconds after IR. Time=min:sec. Images are maximum projections. The movie corresponds to Fig. 4A.
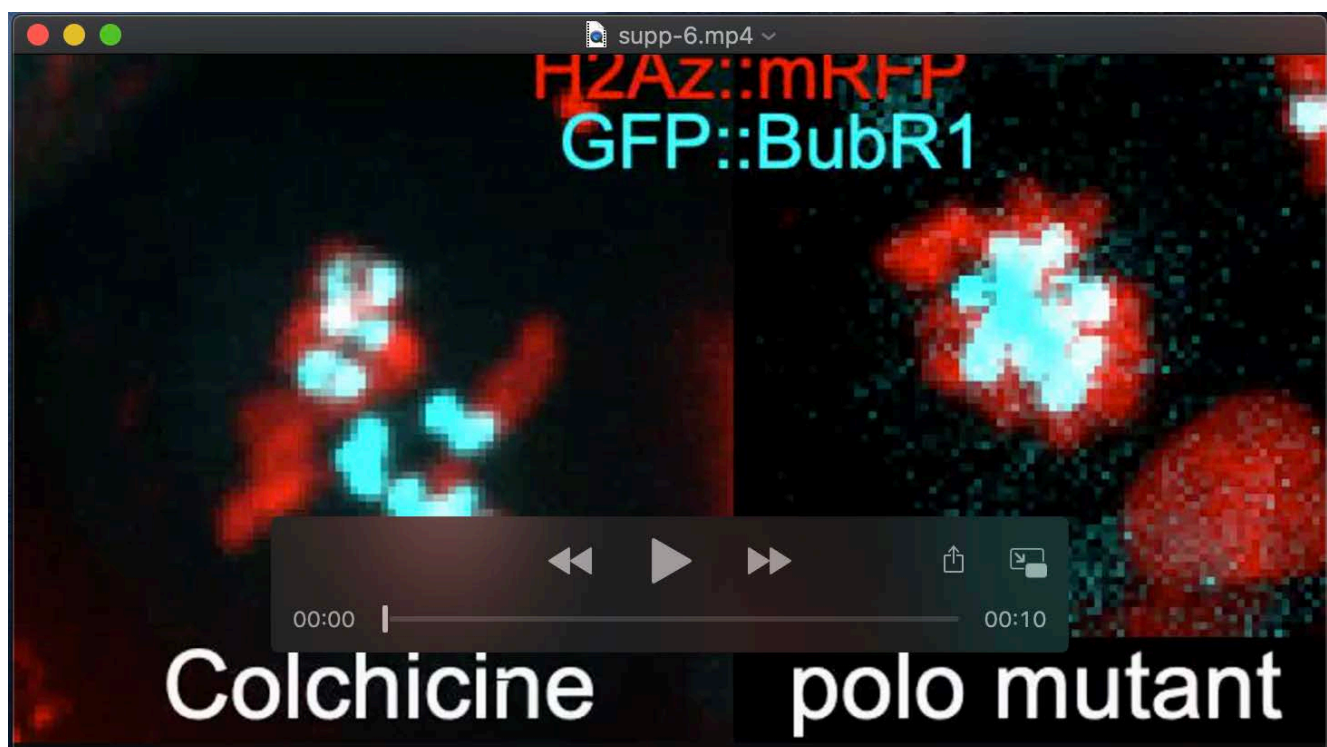
Movie 6: GFP::BubR1 kinetics at mitotic DSBs is altered in *polo* mutant.

Time-lapse video of wild type neuroblast arrested in prometaphase after colchicine treatment (left panel) and *polo*[10] mutant neuroblasts (right panel) expressing H2A.Z::mRFP (red) and GFP::BubR1 (cyan). The first image represents the cells before microirradiation (IR). The yellow arrows point to the site of irradiation (IR). The white arrows indicate the appearance of GFP::BubR1 at the site of damage. Time 0:00 corresponds to the time of recording few seconds after irradiation. Time=min:sec. Images are maximum projections. The movie corresponds to Fig. 5A (top panels).
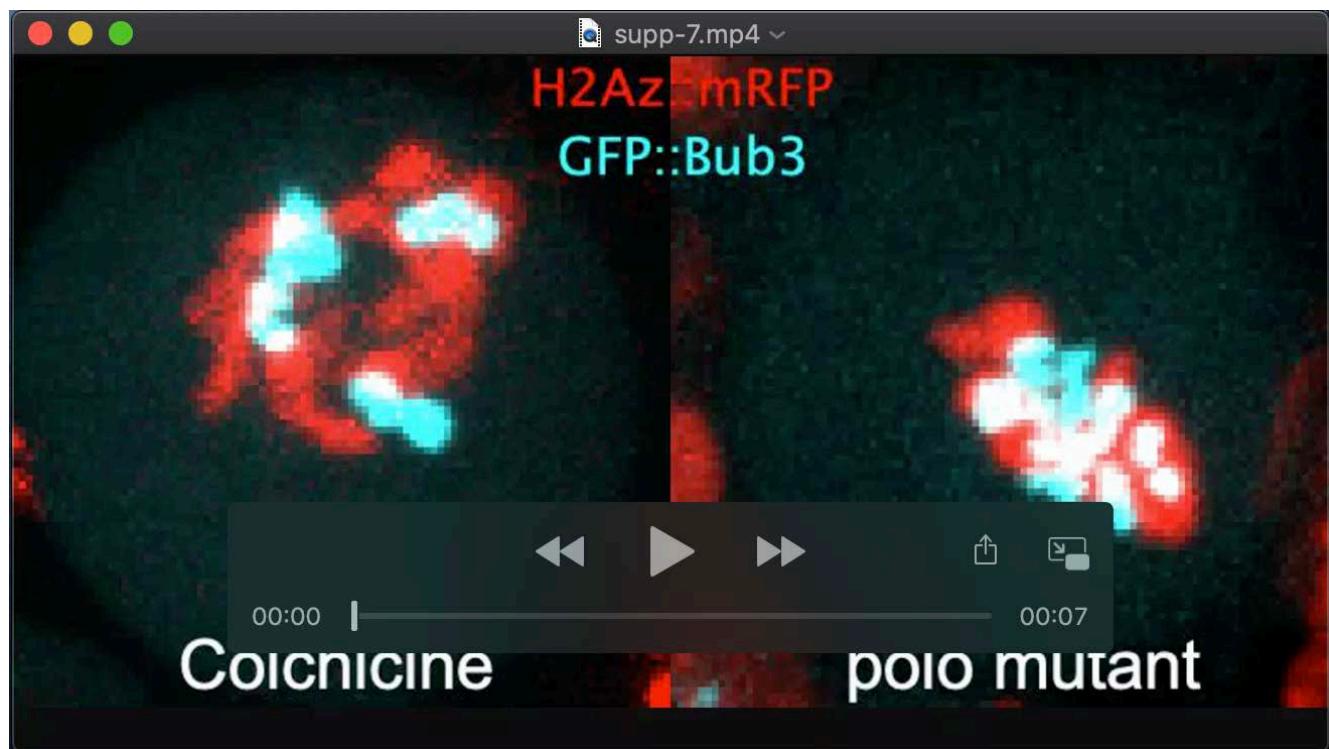
Movie 7: GFP::Bub3 kinetics at mitotic DSBs is altered in *polo* mutant.

Time-lapse video of wild type neuroblast arrested in prometaphase after colchicine treatment (left panel) and *polo*[10] mutant neuroblasts (right panel) expressing H2A.Z::mRFP (red) and GFP::Bub3 (cyan). The first image represents the cells before microirradiation (IR). The yellow arrows point to the site of IR. The white arrows indicate the appearance of GFP::Bub3 at the site of damage. Time 0:00 corresponds to the time of recording few seconds after IR. Time=min:sec. Images are maximum projections. The movie corresponds to Fig. 5A (bottom panels).
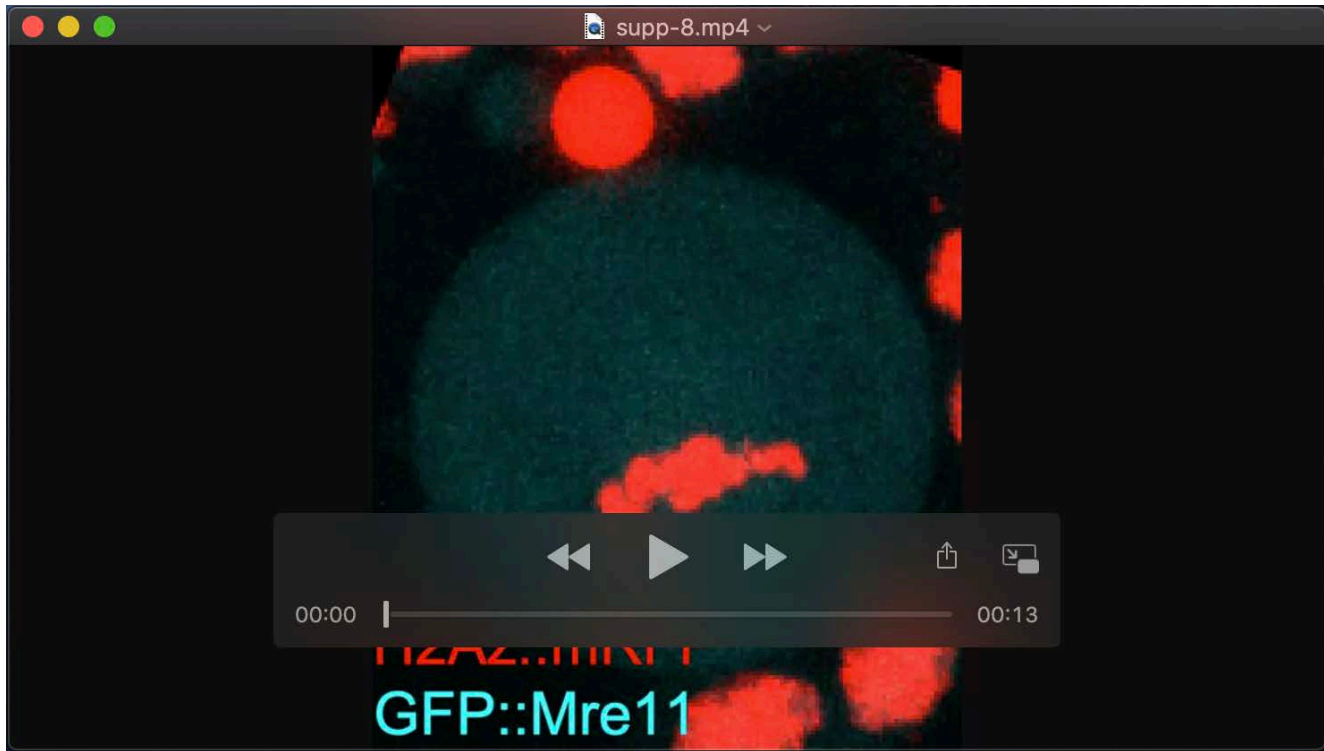
Movie 8: GFP::Mre11 kinetics at mitotic DSBs. Time-lapse video of wild type

neuroblast expressing H2A.Z::mRFP (red) and GFP::Mre11 (cyan). The first image represents

the cell before microirradiation (IR). The yellow arrow points to the site of IR. The white

arrow indicates the appearance of GFP::Mre11 at the site of damage. Time 0:00 corresponds

to the time of recording few seconds after IR. Time=min:sec. Images are maximum

projections. The movie corresponds to Fig. 6A (top panels).

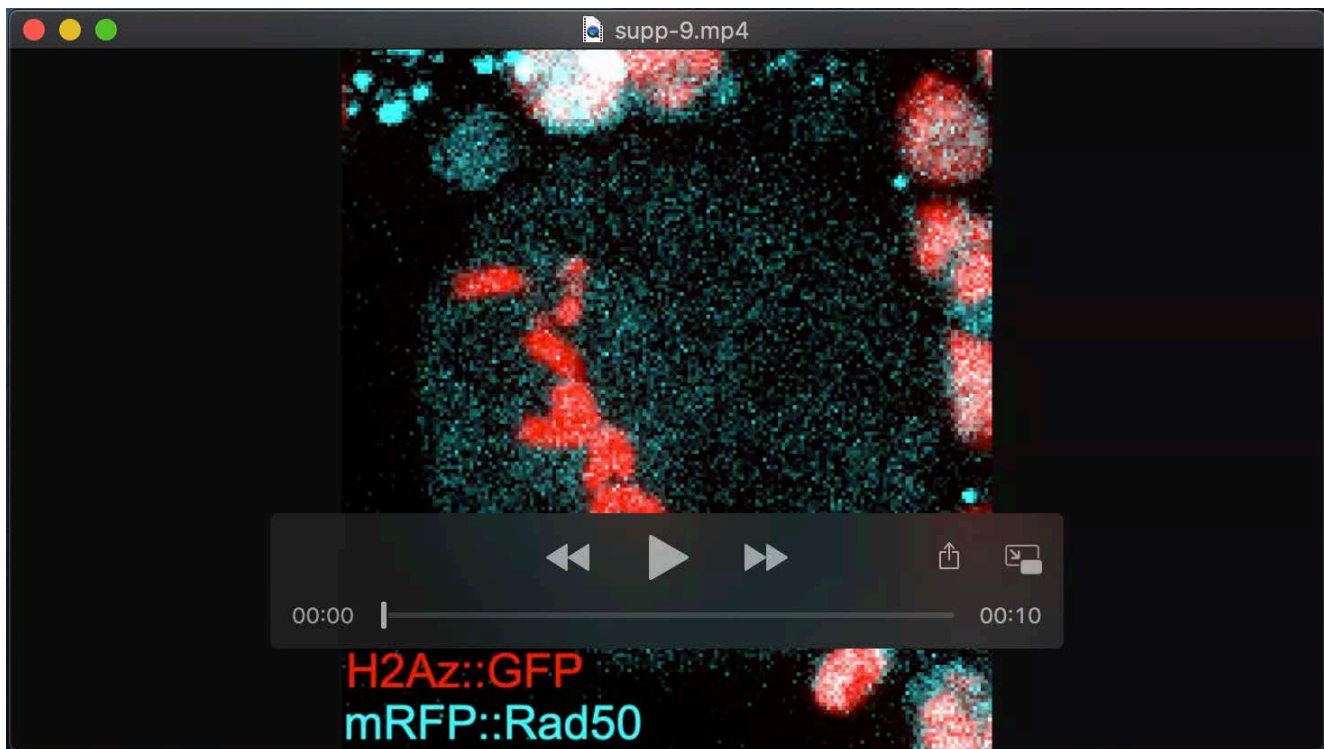
Movie 9: mRFP::Rad50 kinetics at mitotic DSBs. Time-lapse video of wild type neuroblast expressing H2A.Z::GFP (red) and mRFP::Mre11 (cyan). The first image represents the cell before microirradiation (IR). The yellow arrow points to the site of IR. The white arrow indicates the appearance of mRFP::Rad50 at the site of damage. Time 0:00 corresponds to the time of recording few seconds after IR. Time=min:sec. Images are maximum projections. The movie corresponds to Fig. 6A (bottom panels).
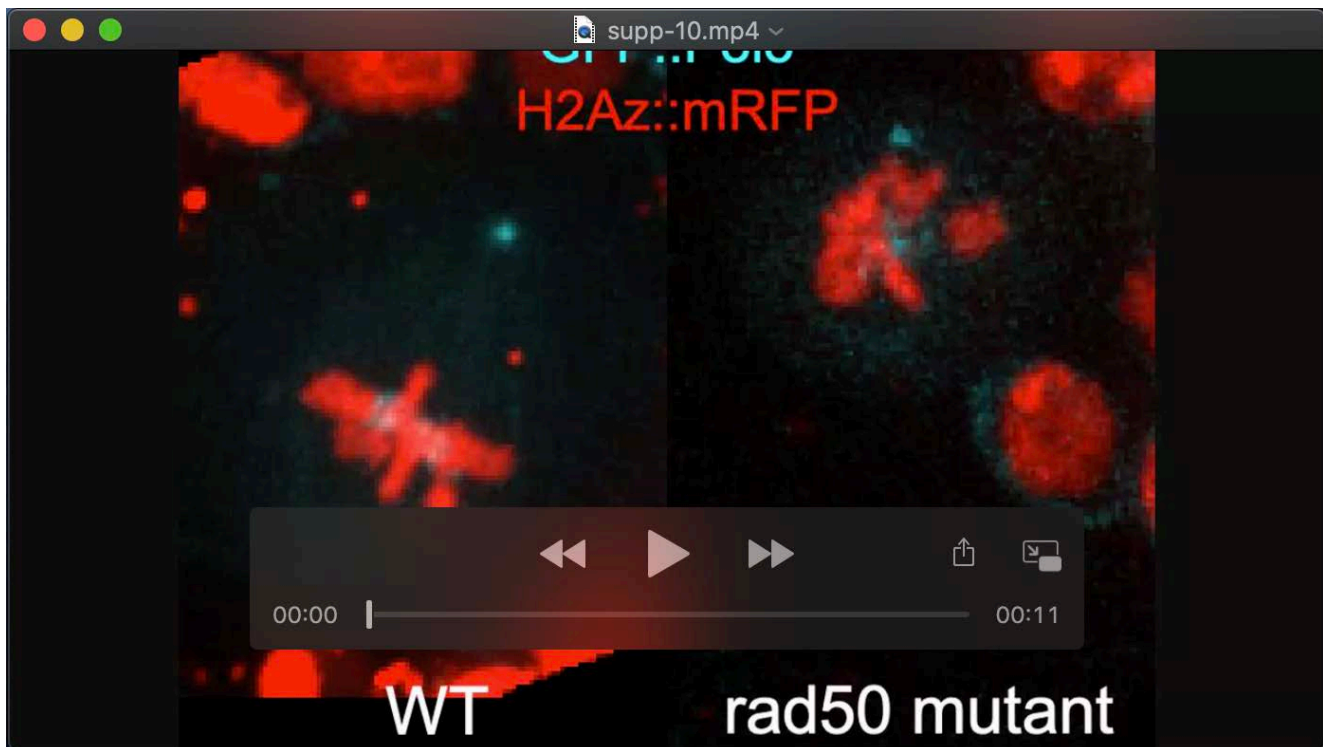
Movie 10: GFP::Polo kinetics at mitotic DSBs is altered in *rad50* mutant.

Time-lapse video of wild type (left panel) and *rad50*^{EP} mutant (right panel) neuroblasts expressing H2A.Z::mRFP (red) and GFP::Polo (cyan). The first image represents the cells before microirradiation (IR). The yellow arrows point to the site of IR. The white arrows indicate the appearance of GFP::Polo at the site of damage. Time 0:00 corresponds to the time of recording few seconds after irradiation. Time=min:sec. Images are maximum projections. The movie corresponds to Fig. 7B.